UNIVERSIDAD DE EXTREMADURA

# TESIS DOCTORAL

# PROCESADO DE NUEVOS MATERIALES COMPUESTOS ULTRADUROS BASADOS EN $B_4C$ MEDIANTE SINTERIZACIÓN POR DESCARGA ELÉCTRICA PULSADA ASISTIDA CON FASE LÍQUIDA TRANSITORIA

CRISTINA OJALVO GUIBERTEAU

**PROGRAMA DE DOCTORADO**
**CIENCIA Y TECNOLOGÍA DE NUEVOS MATERIALES**

**2021**

UNIVERSIDAD DE EXTREMADURA

TESIS DOCTORAL

# PROCESADO DE NUEVOS MATERIALES COMPUESTOS ULTRADUROS DE $B_4C$ MEDIANTE SINTERIZACIÓN POR DESCARGA ELÉCTRICA PULSADA ASISTIDA CON FASE LÍQUIDA TRANSITORIA

CRISTINA OJALVO GUIBERTEAU

PROGRAMA DE DOCTORADO EN
CIENCIA Y TECNOLOGÍA DE NUEVOS MATERIALES

La conformidad de los directores (Ángel Luis Ortiz Seco y Fernando Guiberteau Cabanillas) consta en el original en papel de esta Tesis Doctoral

2021

# UNIVERSIDAD DE EXTREMADURA

ESCUELA DE INGENIERÍAS INDUSTRIALES

DEPARTAMENTO DE INGENIERÍA MECÁNICA, ENERGÉTICA Y DE LOS MATERIALES


# PROCESSING OF NEW ULTRA–HARD $B_4C$ COMPOSITE MATERIALS BY TRANSIENT LIQUID–PHASE ASSISTED SPARK PLASMA SINTERING

**PhD dissertation submitted by Cristina Ojalvo Guiberteau to apply for the degree of Doctor at University of Extremadura**

**Badajoz, 2021**

# ACKNOWLEDGEMENT

First of all, I would like to thank my Thesis directors, Ángel Luis Ortiz and Fernando Guiberteau, for opening the doors to the exciting world of research, which was so unknown to me four years ago. With you I have not only learned new knowledge and experimental techniques but also patience and care for things well done. In addition, you have made me feel like one more of your team from the first day. Thank you, really, for all your effort, respect, and kindness. I would repeat this stage a thousand times.

Thanks to Rodrigo Moreno for having welcomed me so well at the Instituto de Cerámica y Vidrio in Madrid, without forgetting of course Carmen Alcázar, María Díaz, and Marcos Ayllón.

Thanks to Víctor Candelario and Angela Zhang for giving me the opportunity to work with you at the Technical University of Denmark in collaboration with the company LiqTech Ceramics despite the difficulties deriving from the pandemic. Thanks also to María Jiménez for her technical assistance.

Thanks to the Junta de Extremadura for granting me the pre–doctoral contract reference PD16027 corresponding to the call for grants for the training of Doctors in public R&D centres belonging to the Extremadura System of Science, Technology, and Innovation in 2017.

Thanks to the Research Support Services of the UEx, especially to María and Rosario, and to Diego, José, and Uve of the Scientific Material Maintenance and Workshop Service.

Thanks to ADUEx for all the effort you invest in ensuring the well–being of PhD students and, more specifically, for offering me the opportunity to actively participate in the IV Doctoral Conference of the University of Extremadura.

I want to thank the entire Area of Materials Science and Metallurgical Engineering, and especially the GEMA group, for all their help and the experiences I gained from working with them. Thanks Toni for letting me be part of your internship teaching. Thanks to Antonio and Keko for throwing me a lifeline of support in the face of any setback I might have in the laboratory. Claudia, a sister in arms, I am glad that we have met again ten years later. Juanjo, a pleasure to have shared a work desk with you. Aniss, we are left with the promise to ourselves to go to a karaoke, it is pending for when you return. Chico, what a great time we had in Turin. Victor, I think the recovery of your talent for the Area was a great signing, working with you is a joy. Raúl and Jesús, thank you for being so attentive to me.

They say that whoever finds a friend finds a treasure and, without a doubt, mine is one of the most precious treasures I have. María Jesús, always two steps ahead of others, thank you for your advice and, above all, for your friendship. Lola, architect, engineer, and doctor, you know how I admire and appreciate you. Sandra, my favourite "madrileña", thank you for always being there for me. My friends always, Voltia, Marta J., Marta S., Marta V., Piedi, Lola, and Triche, you are unique and essential in my life. Thanks to my friends from college, especially the lights and shades of Cris, Espi, Eli, and Lucía. Manu, thank you for integrating me so well in Madrid, you are a sun. Rosa, my great support during my Erasmus, with you it does not matter the distance that separates us or the time that we have not heard from each other. Auro, an example of overcoming and a source of inspiration, you are a true warrior. Thanks also to Javi G. and especially to Javi C. for their support during the period in Berlin and for encouraging me to embark on this new path. Cris E., thank you for virtually accompanying me on my walks through the Danish capital, I am convinced that you will achieve everything you set your mind to. Óscar, what to tell you that you don't know, thank you for taking care of me, listening to me, and encouraging me to carry on forwards. I am immensely grateful to all of you for believing in me.

Finally, I want to thank the unconditional support of my family: my sisters, Carmen and Patri, my cousin–sister Pili, my brothers–in–law, Nacho and Javi, my precious nephew and niece, Alonso and Carmen, my uncle and aunt, Pedro and Mamen, my cousin Pablo, my grandparents, Diego and Elena, and, of course, my parents, Agustina and Evaristo. Mum and Dad, without you I wouldn't have got this far. I do not have enough words to tell you how I love and admire you. Thank you for your dedication and commitment to us sisters, without a doubt you are the mirror in which I wish to see myself reflected.

# AGRADECIMIENTOS

En primer lugar me gustaría agradecer a mis directores de Tesis, Ángel Luis Ortiz y Fernando Guiberteau, por abrirme las puertas del apasionante mundo de la investigación, que tan desconocido era para mí hace cuatro años. Con vosotros no solo he aprendido nuevos conocimientos y técnicas experimentales sino, también, la paciencia y el cuidado por las cosas bien hechas. Además, habéis conseguido que me sienta como una más desde el primer día. Gracias, de verdad, por todo vuestro esfuerzo, respeto y cariño. Repetiría esta etapa una y mil veces.

Gracias a Rodrigo Moreno por haberme acogido tan bien en el Instituto de Cerámica y Vidrio de Madrid, sin olvidarme por supuesto de Carmen Alcázar, María Díaz y Marcos Ayllón.

Gracias a Víctor Candelario y Angela Zhang por brindarme la oportunidad de trabajar con vosotros en la Universidad Técnica de Dinamarca en colaboración con la empresa LiqTech Ceramics a pesar de las dificultades derivadas de la pandemia. Gracias también a María Jiménez por su asistencia técnica.

Gracias a la Junta de Extremadura por la concesión del contrato predoctoral con referencia PD16027 correspondiente a la convocatoria de ayudas para formación de Doctores en centros públicos de I+D pertenecientes al Sistema Extremeño de Ciencia, Tecnología e Innovación en el ejercicio 2017.

Gracias a los Servicios de Apoyo a la Investigación, en especial a María y a Rosario, y a Diego, José y Uve del Servicio de Taller y Mantenimiento de Material Científico de la UEx.

Gracias a ADUEx por todo el esfuerzo que invertís para velar por el bienestar de los estudiantes de Doctorado y, más concretamente, por dejarme formar parte de las IV Jornadas Doctorales de la Universidad de Extremadura.

Quiero agradecer a todo el área de Ciencias de Materiales e Ingeniería Metalúrgica y en especial al grupo GEMA por toda su ayuda y experiencias vividas. Gracias Toni por dejarme formar parte de tu docencia de prácticas. Gracias a Antonio y Keko por echarme un cable ante cualquier contratiempo que pudiera tener en el laboratorio. Claudia, compañera de batallas, me alegro de que nos hayamos reencontrado diez años más tarde. Juanjo, un placer haber compartido mesa de trabajo contigo. Aniss, nos quedamos con las ganas de ir a un karaoke, queda pendiente para cuando vuelvas. Chico, lo bien que nos lo pasamos en Turín. Víctor, creo que la recuperación de tu talento ha sido un gran fichaje para el área, trabajar contigo es una gozada. Raúl y Jesús, gracias por ser tan atentos conmigo.

Dicen que quien encuentra un amigo encuentra un tesoro y, sin duda, los míos son uno de los tesoros más preciados que tengo. María Jesús, siempre dos pasos por delante de los demás, gracias por tus consejos y, sobre todo, por tu amistad. Lola, arquitecta, ingeniera y doctora, sabes que te admiro y te aprecio. Sandra, mi madrileña favorita, gracias por estar siempre ahí. Mis amigas de siempre, Voltia, Marta J., Marta S., Marta V., Piedi, Lola, Triche, sois únicas e imprescindibles en mi vida. Gracias a mis amigos de la universidad, en especial a las luces y sombras de Cris, Espi, Eli y Lucía. Manu, gracias por integrarme tan bien en Madrid, eres un sol. Rosa, mi gran apoyo durante la Erasmus, contigo no importa la distancia que nos separe o el tiempo que llevemos sin saber la una de la otra. Auro, ejemplo de superación y fuente de inspiración, eres una auténtica guerrera. Gracias también a Javi G. y sobre todo a Javi C. por su apoyo durante mi período en Berlín y por animarme a emprender este nuevo camino. Cris E., gracias por acompañarme virtualmente en mis paseos por la capital danesa, estoy convencida de que conseguirás todo lo que te propongas. Óscar, qué decirte que no sepas, gracias por cuidarme, escucharme y animarme a seguir adelante. Os estoy inmensamente agradecida a todos por creer en mí.

Por último, quiero agradecer el apoyo incondicional de mi familia: mis hermanas, Carmen y Patri, mi prima–hermana Pili, mis cuñados, Nacho y Javi, mis sobrinos preciosos, Alonso y Carmen, mis tíos, Pedro y Mamen, mi primo Pablo, mis abuelos, Diego y Elena, y, por supuesto, mis padres, Agustina y Evaristo. Mamá y papá, no tengo suficientes palabras para deciros lo que os quiero y os admiro. A medida que pasa el tiempo más consciente me hallo de la suerte que tengo de ser vuestra hija. Gracias por vuestra entrega hacia nosotras tres, sin duda sois el espejo en el que deseo reflejarme.

# TABLE OF CONTENTS

# ABSTRACT

The objective of this Doctoral Thesis was to develop new ultra–hard composite ceramics based on $B_4C$, with improved toughness. $B_4C$ has great potential since it has a singular density (~2.52 g/cm$^3$) and hardness (≥30 GPa), and is therefore an excellent candidate to be incorporated into various engineering areas that require components capable of withstanding extreme working conditions (strong contact stresses, high temperatures, aggressive chemical environments, *etc.*). However, its high melting point (~2490 °C), and its inherent brittleness greatly hinders its manufacture and incorporation into these engineering areas. To solve these serious drawbacks, a possible option could be to use small proportions of certain additives that reduce the sintering temperature of the $B_4C$ without compromising its high hardness. The processing of composites based on $B_4C$ therefore represents a challenge worth exploring. Two additives were used in this Doctoral Thesis research, $MoSi_2$ and Ti–Al. These two were chosen because during sintering they generate a transient liquid–phase, which first helps to densify and then reacts in situ with the $B_4C$ disappearing completely to give rise to other refractory and ultra–hard carbides and borides. In addition, to alleviate the problem of the brittleness of $B_4C$, in this Doctoral Thesis ultra–hard and toughened materials were manufactured incorporating carbonaceous nanoplatelets as reinforcements that hinder the propagation of cracks. To obtain these reinforced composite ceramics, two processing routines were developed. The first consisted of homogeneously dispersing the nanoplatelets in the ceramic matrix so that the microstructural reinforcement is isotropic or orthotropic, depending on whether the nanoplatelets are short and randomly arranged or, on the contrary, elongated and oriented in a specific direction. The second consisted of mesostructural design of the material so that it contained layers of nanoplatelets that are equally spaced by about a hundred of microns. All materials were ultra–fast densified by spark plasma sintering (or SPS for short) with or without pressure. Furthermore, many powder mixtures used for SPS with pressure were prepared by aqueous colloidal processing, which was also the technique used for preparing the green parts with near–net–shape for presureless SPS.

# RESUMEN

El objetivo de esta Tesis Doctoral ha consistido en desarrollar nuevos cerámicos compuestos ultraduros basados en $B_4C$, con tenacidad mejorada. El $B_4C$ posee un gran potencial ya que presenta una densidad (~2,52 g/cm$^3$) y dureza (≥30 GPa) singular, y, por ello, es un excelente candidato a incorporarse en diversas áreas de ingeniería que requieren componentes capaces de soportar condiciones extremas de trabajo (fuertes tensiones de contacto, temperaturas elevadas, ambientes químicos agresivos, etc.). No obstante, su elevada temperatura de fusión (~2490 ºC), y su inherente fragilidad dificulta enormemente su fabricación e incorporación a dichas áreas de ingeniería. Para resolver estos serios inconvenientes una posible opción podría ser añadir pequeñas proporciones de ciertos aditivos que consigan reducir la temperatura de sinterización del $B_4C$ sin comprometer su elevada dureza. Por tanto, el procesado de materiales compuestos basados en $B_4C$ representa un desafío que merece la pena explorar. En esta Tesis Doctoral se han utilizado dos aditivos, el $MoSi_2$ y el Ti–Al. Se han escogido estos dos porque durante la sinterización generan una fase líquida transitoria, que primero ayuda a densificar y luego reacciona in situ con el $B_4C$ desapareciendo completamente para dar lugar a otros carburos y boruros también refractarios y ultraduros. Además, para paliar el problema de la fragilidad del $B_4C$, en esta Tesis Doctoral se han fabricado materiales ultraduros y tenaces incorporando nanoplaquetas carbonosas como refuerzos que dificultan la propagación de fisuras. Para obtener estos cerámicos compuestos reforzados se han desarrollado dos rutas de procesado. La primera de ellas ha consistido en dispersar homogéneamente las nanoplaquetas en la matriz cerámica de forma que el refuerzo microstructural sea isotrópico u ortotrópico, dependiendo de si las nanoplaquetas son cortas y están dispuestas al azar o, por el contrario, son alargadas y están orientadas en una dirección concreta. La segunda ha consistido en el diseño mesoestructural del material de forma que contuviera capas de nanoplaquetas equiespaciadas entre sí a una distancia cercana a la centena de micras. Todos los materiales se densificaron de manera ultrarrápida mediante sinterización por descarga eléctrica pulsada (abreviado como SPS por sus siglas en inglés) con o sin presión. Además, muchas mezclas de polvos usadas para SPS con presión se prepararon a su vez mediante procesado coloidal acuoso, que fue también la técnica empleada para preparar materiales verdes con casi forma final para SPS sin presión.

# CHAPTER 1

# Introduction and statement of purpose

The continuous development of new industrial applications requires the increasing use of new materials to satisfy the demand for ever more stringent properties. Two large groups of materials are usually distinguished according to what they are needed for, *i.e.*, functional and structural materials. Technical ceramics are used mainly in functional applications due to their special electrical, optical, thermal properties, *etc.*, while metallic materials are the most used for structural purposes due to their excellent combination of mechanical properties (where their toughness stands out). However, it should be emphasized that the advantages of metallic materials disappear at high temperatures and/or in chemically aggressive environments due to the degradation (oxidation, corrosion, *etc.*) that they experience in such adverse working conditions. Thus, technical ceramics remain as the only possible alternative. In addition, ceramic materials can also be the best option at room temperature in those applications that require high resistance to wear and contact damage such as sliding or ball bearings, cutting tools, *etc.*, as well as elements protecting against ballistic impact (armours, bullet–proof vests, *etc.*), because they are harder and lighter than metallic materials.

Ceramic materials are the result of the combination of metallic and non–metallic chemical elements joined together by strong ionic–covalent bonds. In terms of their composition, two large groups of ceramics are usually distinguished, oxidic ($SiO_2$, $Al_2O_3$, $ZrO_2$, *etc.*) and non–oxidic, such as carbides, borides and nitrides (SiC, $ZrB_2$, $Si_3N_4$, *etc.*). In general, they are materials with high melting points and very low diffusion coefficients, which makes their manufacture difficult. A second drawback is that, although they are rigid and hard materials, they are also brittle, which limits their usefulness in structural applications. The third drawback that ceramic materials generally have for them to be used in industrial applications is the difficulty in machining them, precisely due to their hardness and brittleness.

Boron carbide ($B_4C$) is the hardest material that can be manufactured on an industrial scale since, while its hardness (≥30 GPa) is only surpassed by diamond and cubic boron nitride, $B_4C$ can indeed be synthesized in large quantities. This and its low density (~2.52 g/cm$^3$) make it an ideal candidate for many industrial applications, especially those that require high resistance against wear and, in general, contact damage. However, as mentioned above, elevated temperatures and long

sintering times are required to achieve fully dense $B_4C$. Also the inherent brittleness of this material compromises its integrity under service conditions, especially when it is subject to strong and prolonged contact stresses. Finally, due to its extreme hardness and fragility, dense $B_4C$ is very expensive or unfeasible to machine, which is why there is a need for processing routes that allow the manufacture of near–net–shape parts.

The main motivation of this Doctoral Thesis is precisely to advance in knowledge towards solving the aforementioned difficulties. Specifically, this study had four main objectives:

1. To make new $B_4C$–based composite materials at lower temperatures and for shorter times, in order to reduce production costs.
2. To develop environmentally respectful processing routes to manufacture dense near–net–shape parts, thus minimizing the costly, tedious, and risky tasks of machining.
3. To optimize the wear resistance of these materials, designing and developing microstructures that are suitable for this purpose.
4. To fabricate new materials with microstructures that exhibit toughness reinforcement mechanisms, in order to increase their fracture resistance.

A wide variety of strategies were used to achieve these objectives. They included the following:

- Incorporation of sintering additives to reduce the manufacturing temperature, but without excessively compromising the hardness of the material. The strategy followed consists of using suitable additives that generate a transient liquid–phase during sintering. With this, not only is a liquid–phase formed to facilitate densification during sintering, but also it is then completely consumed by reacting with the $B_4C$, giving rise to second phases (carbides and borides) with a hardness that is also high. Specifically, the additives used in this Doctoral Thesis were a ceramic ($MoSi_2$) and an intermetallic (Ti–Al).
- Use of the ultra–fast spark plasma sintering (SPS) technique to achieve fine–grained microstructures, and therefore materials with optimized hardness. This strategy avoids slow heating ramps that promote grain growth versus densification, as is unfortunately the case in conventional sintering. The simultaneous application of pressure during heating in the SPS technique also favours densification. Thus, the use of SPS provides a twofold benefit by substantially reducing manufacturing temperatures by 200–300 °C and allowing microstructures to be obtained that are unattainable by conventional

sintering.

- Use of aqueous colloidal processing to manufacture near–net–shape parts. The preparation of highly concentrated ceramic suspensions in water is a great challenge, and in addition represents a major advance in the line of the research carried out to date since this processing method is more respectful with the environment. In particular, it is harder to form a dispersion of particles in an aqueous medium than in alcohol due to water's greater surface tension. This is especially so when the particle concentrations required are high. Furthermore, in the present case, $B_4C$ and its additives are non–oxidic, and therefore oxidize in water. The problem is even more complicated if one takes into account that it is not only a matter of dispersing particles but also of homogenizing mixtures of different kinds.
- Incorporation of carbonaceous phases into the microstructure of the materials developed so as to increase their toughness. The strategy is to incorporate two–dimensional nano–structures (*i.e.*, nanoplatelets) because they disperse more readily than one–dimensional ones (*i.e.*, nanotubes). In addition, they are more effective in bridging and redirecting cracks. In this work, both graphene oxide (GO) and partially reduced graphene oxide (prGO) nanoplatelets were used, but in both cases with the idea of obtaining reduced graphene oxide (rGO) nanoplatelets after sintering.
- Fabrication of $B_4C$–based materials with nanometric grain size to optimize their hardness and wear resistance. The strategy is to use $B_4C$ starting nanopowders in combination with the SPS technique to minimize grain growth during densification. Only in this way is it possible to finally obtain a dense and nanostructured $B_4C$ material.

The rest of this Thesis report is organized as follows:

Chapter 2 is dedicated to the "State of the Art" and deals with the advances and challenges posed by the development of new $B_4C$–based ceramic materials. It begins in Subchapter 2.1 by presenting this compound's properties and crystalline structure. Subchapter 2.2 presents a bibliographic review of the most relevant studies available on the processing and mechanical properties of $B_4C$ ceramics.

From Chapters 3 to 10, the results of the work carried out in this Doctoral Thesis are presented, analysed, and discussed. These results have been published or submitted in articles in the Journal of the European Ceramic Society during the period "2019–2021", but they are not necessarily described in chronological order. In all cases, these are studies aimed at the development, fabrication, and

characterization of new ultra–hard $B_4C$–based materials. The first two chapters correspond to work carried out using $MoSi_2$ as sintering additive, while the remaining six correspond to the use of Ti–Al.

Chapter 3 presents the results of a first study on sintering and characterization of new composite $B_4C$–based materials with different proportions of $MoSi_2$ additive (5, 10, and 15 vol.%). This work was the first time that the manufacture of these materials using the SPS technique had been explored.

Chapter 4 is the logical continuation of the previous one, since it is aimed at determining the ideal proportion of additives to achieve materials with optimized hardness and toughness, expanding the proportions of $MoSi_2$ to 20, 25, and 30 vol.%. The results of a detailed study of the most optimal material's dry wear resistance are included, comparing it with that of a reference $B_4C$ ceramic manufactured under the same conditions and with that of other $B_4C$ ceramics and compounds.

In Chapter 5, the wear resistance is studied of the composite material manufactured with the mixture of powders of $B_4C$ and Ti–Al (5 vol.%), also densified by SPS, again for comparison with that of a $B_4C$ reference manufactured under the same conditions and with that of another manufactured at a much higher temperature.

Chapter 6 focuses on the description of an aqueous colloidal processing route that was developed to co–disperse $B_4C$ and Ti–Al particles (5 vol.%) to obtain both powder mixtures and near–net–shape parts, in both cases for subsequent densification by SPS either with or without the simultaneous application of pressure. The main objective of this study was to determine the optimal conditions for obtaining concentrated suspensions of particles (30 vol.% solid) that are, on the one hand, homogeneous and, on the other, sufficiently fluid to be cast into moulds with complex shapes.

Once demonstrated the viability of aqueous colloidal processing and the advantages of the SPS technique to manufacture the composite materials described above, the interest is focused on developing new materials that may be useful in industry. This implied obtaining microstructures that are wear resistant because that is the property to be exploited, and that have improved toughness because that is the main problem to resolve. So, Chapter 7 presents the results of a detailed study of the influence of grain size on the dry wear resistance of $B_4C$ composites manufactured with Ti–Al (5 vol.%), covering the nano– to the micro–metre range. To manufacture these materials, it was necessary to first adjust the colloidal processing conditions that

allow the dispersion of particles of different sizes, especially in the case of nanometric particles, and the SPS conditions that retain the nanostructure.

Chapters 8, 9, and 10 correspond to work in which the focus was on the manufacture of composite materials of $B_4C$ with Ti–Al additives that, in addition, contain reinforcements (graphene oxide) to improve their microstructure's toughness.

Chapter 8 corresponds to the first work done using GO nanoplatelets (10 μm diameter and 0.005 μm thickness) and prGO (5 μm diameter and 0.002 μm thickness). The most suitable aqueous colloidal processing conditions to disperse these $B_4C$+Ti–Al+GO/prGO mixtures were determined. With GO nanoplatelets, the simultaneous application of pressure during sintering causes them to align in the direction perpendicular to the load axis, and therefore the resulting microstructure is reinforced orthotropically. However, with prGO nanoplatelets, there is no definite preferential orientation to their alignment, leading to isotropically reinforced microstructures.

In Chapter 9 the focus is on the fabrication of materials reinforced with rGO nanoplatelets that are isotropic and near–net–shaped. For this reason, not only are small–sized rGO nanoplatelet reinforcements used, but also SPS densification is performed without applying pressure in order to preserve the original shape of the part.

In Chapter 10, the goal is to achieve mesostructured orthotropic microstructures. Laminated materials are prepared with alternating layers of $B_4C$+Ti–Al and rGO, approximately 100 μm and 2–3 μm thick, respectively. For this, individual sheets of $B_4C$+Ti–Al were manufactured by means of aqueous colloidal processing and tape casting. They were subsequently coated with suspensions of $B_4C$+Ti–Al with a high solid content of rGO. The sheets thus manufactured were stacked and punched for their densification by means of SPS with simultaneous application of pressure.

Finally, and in accordance with the Regulations for Doctoral Studies of the University of Extremadura, Chapter 11 summarizes the main results, and Chapter 12 and 13 presents the most relevant conclusions and implications to be drawn from this Doctoral Thesis.

# CHAPTER 2

# State of the art

## 2.1. Boron Carbide. Properties and Crystalline Structure

Refractory carbides are materials with melting points above 1800 °C and are characterized by their great chemical stability [1]. Two types of carbides are usually distinguished – the interstitials that result from the combination of C with a transition metal (groups IVB, VB, and VIB), and the covalents that are obtained when C forms a combination with B or Si. The interstitial carbides are arranged so that the carbon atoms occupy the interstitial voids in the compact structures of the transition metal, which is possible because the atomic radius of C is much less than that of the metal. The electronegativity of C is much greater than that of metals, so that in interstitial carbides are bonded by a mixture of metallic, covalent, and ionic bonds. The case of covalent carbides is completely different. The electronic configuration of the two elements is similar because they are very close in the periodic table, and so therefore are their atomic radii and electronegativities. The bond is therefore essentially covalent, *i.e.*, the C and Si (or B) atoms share electrons. **Table 2.1** lists the electron configurations of these three elements.

**Table 2.1.** Electron configurations of B, C, and Si [1].

| Element | Z# | Electron configuration | Electronegativity | Atomic radius (nm)* |
|---|---|---|---|---|
| **Boron** | 5 | $[He]2s^2p^1$ | 2.0 | 0.088 |
| **Carbon** | 6 | $[He]2s^22p^2$ | 2.5 | 0.077 |
| **Silicon** | 14 | $[Ne]3s^23p^2$ | 1.8 | 0.117 |

# Z denotes the atomic number.
* In tetrahedral configuration ($sp^3$ hybridization).

**Table 2.2** compares some properties of various refractory carbides, both covalent and interstitial. As can be seen, boron carbide has a unique combination of properties since, although it is the least refractory, it has the highest hardness values and is the lightest. Indeed, its hardness is only exceeded by diamond and cubic boron nitride, which it surpasses in its capacity for production on an industrial scale. Given its colour, it is often called the "black diamond" [2,3]. In the last decades, it has

attracted the attention of numerous researchers due to its potential for applications that require great rigidity, hardness, and wear resistance, even at elevated temperatures. It is also used as a high–temperature semiconductor [1–5].

Table 2.2. Properties of some refractory carbides [1].

| MATERIAL | | | Density ($g/cm^3$) | Melting point (°C) | Vickers hardness (GPa) | Young's modulus (GPa) | Thermal conductivity at 20°C (W/m·K) |
|---|---|---|---|---|---|---|---|
| Interstitial carbides | IV | TiC | 4.91 | 3067 | 28–35 | 410–501 | 21 |
| | | ZrC | 6.59 | 3420 | 25.9 | 350–440 | 20.5 |
| | | HfC | 12.67 | 3928 | 26.1 | 350–510 | 20 |
| | V | VC | 5.65 | 2830 | 27.2 | 430 | 38.9 |
| | | NbC | 7.79 | 3600 | 19.6 | 338–580 | 14.2 |
| | | TaC | 14.5 | 3950 | 16.7 | 285–560 | 22.1 |
| | VI | $Mo_2C$ | 9.06 | 2520 | 15.5–24.5 | 535 | 21.5 |
| | | WC | 15.8 | 2870 | 22 | 620–720 | 63 |
| Covalent carbides | | SiC [6] | 3.2 | 2650–2950 | 23–25 | 410 | 150–200 |
| | | $B_4C$ | 2.52 [2] | 2490 [10] | 31 [7]–39 [8] | 448 [2] | 20–35 |

Boron carbide has been the subject of numerous investigations aimed at deciphering its complex crystal structure [2–5,9–12]. Although it is generally designated as $B_4C$, unlike SiC, it is not actually defined with any given stoichiometry. The B–C phase diagram **(Fig. 2.1)** clearly reflects this fact, since it shows how boron carbide actually corresponds to an intermediate domain, *i.e.*, its atomic percentage of C is variable. The limits of this domain are still unclear because, although there is some agreement that the minimum atomic percent of C is approximately 8.8% [2,4,10,11], atomic percents of 18.8%, 20%, and 21.6% have been proposed as upper limits [2,3,5,10,11]. The stoichiometries that delimit the stability domain of boron

carbide in the diagram of **Fig. 2.1** are approximately $B_{10.5}C$ and $B_4C$. Boron carbide only exists in equilibrium with C at the upper limit, while for values higher or lower than the stability domain it coexists with free boron or graphite, respectively. The melting point is approximately 2490 °C, and, as shown in **Fig. 2.1**, for percents close to 13% melting occurs directly, *i.e.*, without passing through a prior two–phase solid–liquid domain. However, when the carbon content approaches the limiting values, formation of the liquid–phase begins at notably lower temperatures.

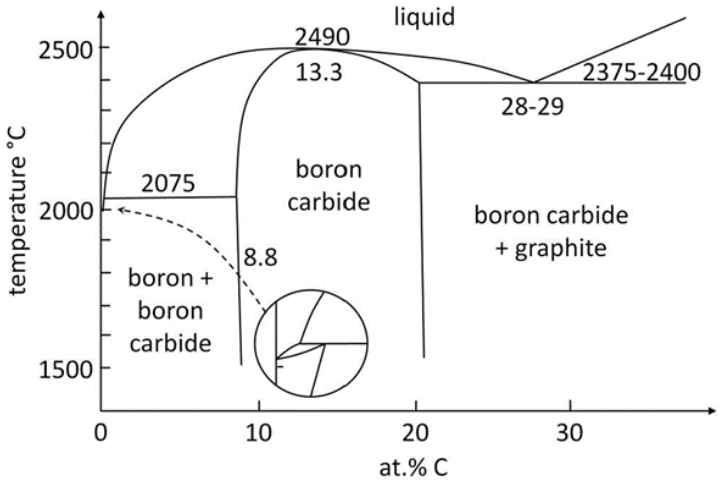


**Figure 2.1.** Boron carbide phase diagram [10].

The crystalline structure of boron carbide is much more complex than that of silicon carbide, among other reasons because both C and Si require 4 electrons to complete their valence shell, while B requires 5 (**Fig. 2.2a**). In the three types of atoms, the orbitals hybridize in such a way that B passes from 1 to 3 valence electrons, while C and Si pass from 2 to 4 (**Fig. 2.2.b**). In both C and Si, the 2s orbital hybridizes with the three p orbitals to form four hybrid $sp^3$ orbitals. Thus, each Si atom can bond to four C atoms in a tetrahedral arrangement and vice versa. In SiC therefore, there is only a single type of bond (C–Si), and the different possible ways of stacking these tetrahedra give rise to the different polymorphic variants exhibited by this compound [13]. In B, the 2s orbital hybridizes with one or two 2p orbitals, generating hybrid sp and $sp^2$ orbitals. There thus result four orbitals, but only three of them have an electron available to bond with another, while the fourth is empty. Hence B can accept pairs of electrons to complete the unoccupied fourth orbital, tending to form multi–centred bonds. For the reasons given, in boron carbide it is not possible to obtain crystalline structures only with C–B bonds, with C–C and B–B bonds also being necessary, as will be seen below.

(a)

| E* | Z | K | L | | | | M | | | |
|---|---|---|---|---|---|---|---|---|---|---|
| | | 1s | 2s | 2px | 2py | 2px | 3s | 3px | 3py | 3pz |
| B | 5 | ↑↓ | ↑↓ | ↑ | | | | | | |
| C | 6 | ↑↓ | ↑↓ | ↑ | ↑ | | | | | |
| Si | 14 | ↑↓ | ↑↓ | ↑↓ | ↑↓ | ↑↓ | ↑↓ | ↑ | ↑ | |

(b)

| E* | Z | K | L | | | | M | | | |
|---|---|---|---|---|---|---|---|---|---|---|
| | | 1s | 2s | 2px | 2py | 2pz | 3s | 3px | 3py | 3pz |
| B | 5 | ↑↓ | ↑ | ↑ | ↑ | | | | | |
| C | 6 | ↑↓ | ↑ | ↑ | ↑ | ↑ | | | | |
| Si | 14 | ↑↓ | ↑↓ | ↑↓ | ↑↓ | ↑↓ | ↑ | ↑ | ↑ | ↑ |

*E denotes element

**Figure 2.2.** (a) Configuration of the electron shells of B, C, and Si.
(b) hybridization $sp^2$ of boron (yellow) and $sp^3$ of carbon and silicon (blue) [1].

Therefore, due to its diverse stoichiometry and the peculiarities of B, the organization of the atoms in boron carbide is complex and varied. However, it usually responds to an $X_{12}XXX$ pattern in which $X_{12}$ represents 12 atoms that occupy the corners of an icosahedron, as is the case in pure boron, and XXX represents a 3–atom chain [5]. With this pattern, the only two ordered structures possible are $B_{12}CCC$ and $B_{12}CBC$ [5], whose C atom percents are 20% and 13.3%, respectively.

The crystal structure of $B_{12}CCC$ has B icosahedra centred at the corners of a rhombohedral cell (a = 5.16 Å, α = 65.7°) [5], and a C chain in the centre aligned in the [111] direction (**Fig. 2.3a**). In elemental B, the atoms also occupy the vertices of icosahedra centred at the corners of a rhombohedral cell, so conceptually one may consider that the $B_{12}CCC$ structure is obtained by introducing a C chain in the centre of the B cell (**Fig. 2.3b**), with the consequent modification of the cell parameters.

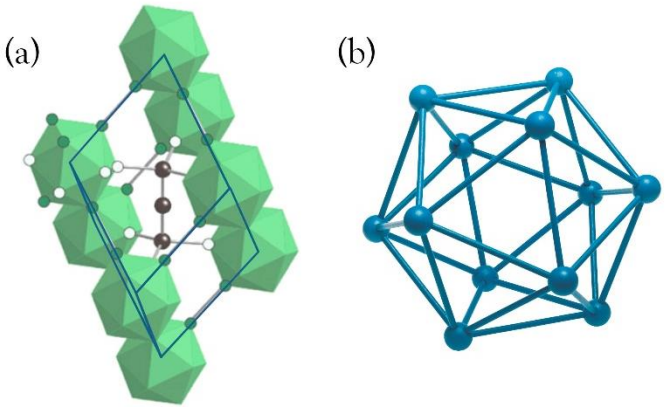


**Figure 2.3.** (a) Boron carbide unit cell based on icosahedra and a chain [10].
(b) Rhombohedral structure of boron.

In the $B_4C$ structure, the icosahedra are oriented so that the three B atoms of the same triangular face are each located on an edge of the cell, and at the same distance from the vertex **(Fig. 2.4)**. Therefore, the direction [111] of the rhombohedral cell is always perpendicular to a pair of parallel faces of the icosahedron. As noted above, the central atom of the C chain is located at the centre of the cell, and the other two at the same distance from it in the [111] direction. The structural base thus comprises 15 atoms, 12 of B and 3 of C, so that the formula or stoichiometric ratio is $B_4C$.

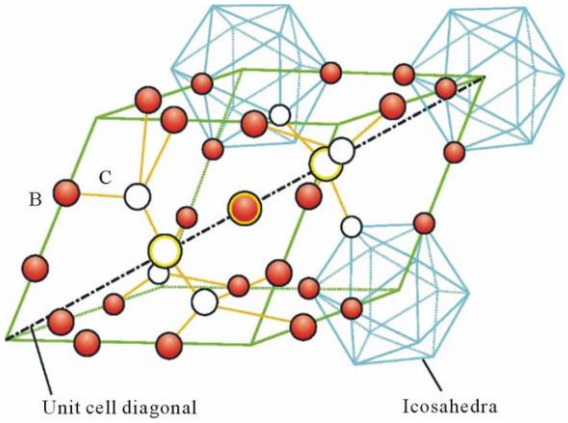


**Figure 2.4.** Boron carbide unit cell [14].

Focusing now on the coordination existing in the structure described above, *i.e.*, the bonds between the different atoms, one sees that the B atoms occupy two types of sites in the icosahedron, polar and equatorial [3]. The six polar sites are the corners of the triangular faces perpendicular to the [111] direction. The six equatorial sites are the remaining vertex of the icosahedron. They form a hexagonal "chair" **(Fig. 2.5)**.

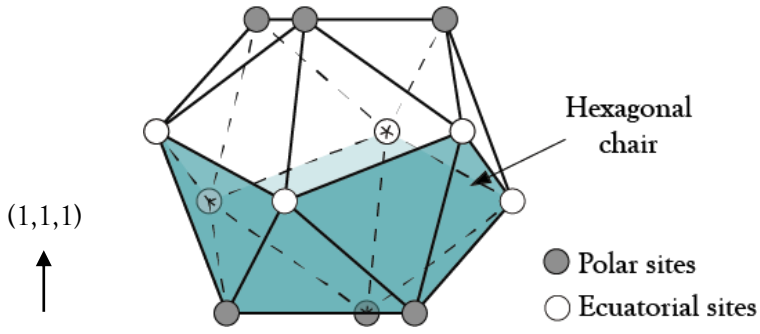


**Figure 2.5.** Positions of the B atoms in the icosahedron.

The C atoms also occupy two types of site, the centre and the ends of the chains. As illustrated in **Fig. 2.6**, the polar–site B atoms in the the $B_{12}CCC$ structure bind to six other B atoms, five in the same icosahedron (two at polar sites and three at equatorial sites) and the sixth in a neighbouring icosahedron (also at a polar site). However, the equatorial–site B atoms bind to five others in the same icosahedron (three at equatorial sites and two at polar sites) as well as to a C atom at the end of a chain. Finally, the only links of the central atom of each C chain are to the other two at the ends. In sum, all the B atoms are linked to a total of six atoms, while the C atoms are linked to either two or four, depending on whether they are in the centre or at the ends of the chain, respectively. It is therefore a structure formed by B icosahedra and C chains in which each icosahedron is linked to both six icosahedra (polar atoms) and six chains (equatorial atoms), while each chain is linked to just six icosahedra.

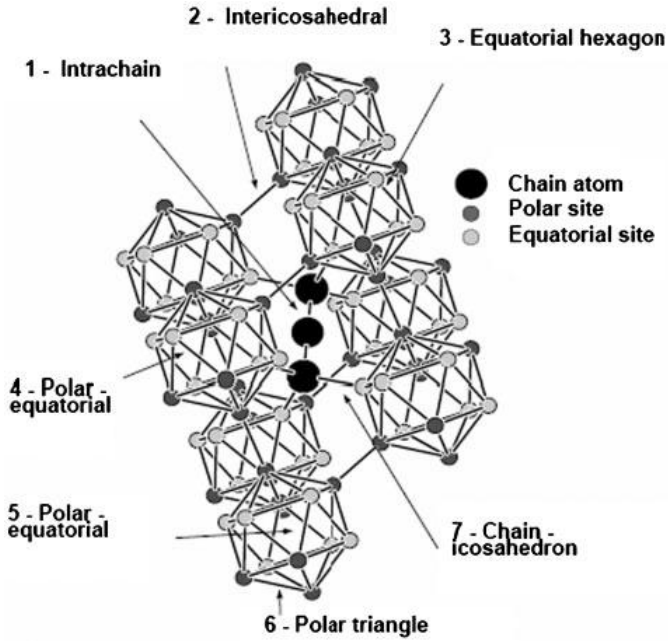


**Figure 2.6.** Types of sites and bonds in the boron carbide unit cell [2].

Thus, in this structure four types of bonds are distinguished. From shortest to longest they are [5]: *(i)* intra–chain C–C, *(ii)* chain–icosahedron C–B, *(iii)* inter–icosahedral B–B, and *(iv)* intra–icosahedral B–B. In other words, the strongest bonds are those that link the atoms of a chain, followed by those that join a chain to the nearest icosahedra. The weakest are those that link the B atoms of the same icosahedron, followed by those linking the icosahedra.

The $B_{12}CCC$ crystal structure can also be described by a hexagonal cell whose [0001] direction coincides with the [111] direction of the rhombohedral cell (**Fig. 2.7**). As can be seen, the hexagonal cell contains three chains and three icosahedra, so that it contains the structural base three times, *i.e.*, a total of 45 atoms (36 B and 9 C). The volume of the hexagonal cell is thus three times that of the rhombohedral cell.

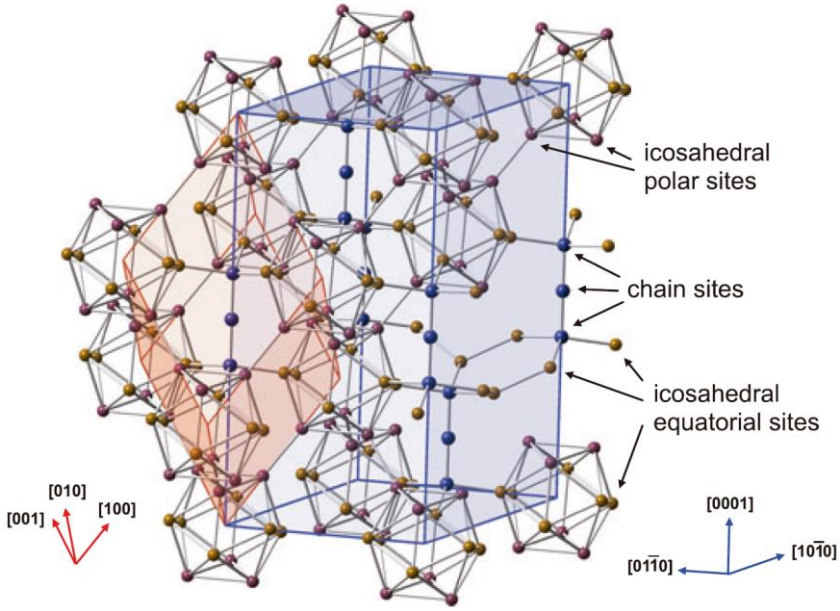


**Figure 2.7.** Rhombohedral (red) unit cell and hexagonal (blue) multiple cell of boron carbide [5].

If the C atom in the centre of the chain in the $B_{12}CCC$ structure is replaced by B, one gets the $B_{12}CBC$ ordered structure. With this modification, the C atom percent falls from 20% to 13.3%. Substitution of another C atom by B would be impossible because this would reduce the atom percent to 6.6%, outside boron carbide's stability domain. Although the only two ordered structures $B_{12}CCC$ and $B_{12}CBC$ correspond to the stoichiometries $B_4C$ (20 at.% C) and $B_{6.5}C$ (13.3 at.% C), respectively, this does not mean that the inverse is necessarily the case. Indeed, the belief that $B_4C$ is formed by icosahedra of B and chains of C has been discarded since successive refinements of experimental models have shown that C atoms can also occupy the B sites and vice versa [2–5,9–12].

In the B–C phase diagram (**Fig. 2.1**), the $B_4C$ stoichiometry is very close to the upper limit of the boron carbide stability domain, while $B_{6.5}C$ is close to the central zone. Thus in general, the structure of boron carbide can be considered to be either that of $B_{6.5}C$ modified to contain more or less C, or that of $B_4C$ modified to contain

less C. The latter interpretation is consistent with the fact that the formula $B_4C$ is always used to refer to this compound, regardless of its actual C content.

In view of the foregoing, one can state that in general there is an intrinsic disorder in boron carbide that gives rise to a great many polymorphic variants. In the case of $B_4C$ for example, a total of 52 polymorphs forming 10 different families have been recognized [12], with $B_{11}$CCBC being the most abundant disordered structure [2–3,5,9–12]. The main difficulty with the different structural model proposals is to locate precisely the positions of B and C in the crystalline structure, since these atoms are so close in the periodic table that their (nuclear and electron) scattering cross–sections are very similar [2,10].

With regard to the composition of the icosahedra, it is generally accepted that with increasing carbon content there is a progressive change from $B_{12}$ to $B_{11}C$, $B_{10}C_2$, and $B_9C_3$ [3,5], with the C atoms preferentially occupying the polar sites [2,4]. There is far more controversy about the composition and organization of the chains since, although CBC is the most widely accepted configuration, some authors [2–5,9–12] claim that there is a certain percentage of chains such as CCC, CCB, CBB, BCB, and BBB, as well as others with vacancies, forming rings, *etc*. Some authors also argue that the bonds in the chains are not strongly covalent since the end atoms are weakly linked to the central atom which, moreover, tends to shift in the direction perpendicular to the ternary axis, and they even raise the idea that the central atom, generally of B, is actually an ion [5,9] compressed between the ends of the chain and that, therefore, it tends to occupy interstitial positions in the crystalline structure [4,9]. Therefore, the configuration of the chains is a clearly complex issue that requires much further analytical effort. **Fig. 2.8** shows high–resolution electron microscopy images corresponding to single crystals with the stoichiometry $B_{13}C_2$. Based on the observations made, the following chain models have been posited [3]: *(i)* four–atom chains combined with straight CBCs, *(ii)* chains with vacancy defects C□C (where □ is a vacancy), *(iii)* bent CBCs oriented differently from the singular chains relative to the projected direction, *(iv)* straight chain combined with a $CB_2C$ rhombus, *(v)* bent chains combined with $CB_2C$ rhombi, and *(vi)* $CB_2C$ rhombi. Therefore, even for a stoichiometry that is compatible with the $B_{12}$CBC ordered structure, six different chain patterns have been observed.

To end, **Fig. 2.9** is a plot of the hexagonal cell parameters as a function of the boron carbide's C content. As can be seen, the parameter a decreases progressively as the C content increases, while the parameter c remains constant up to approximately 13 at.% C, after which its decrease is even sharper than that of parameter a. Thus,

the cell size in general decreases with increasing C content due to the progressive replacement of B atoms by the smaller C atoms.

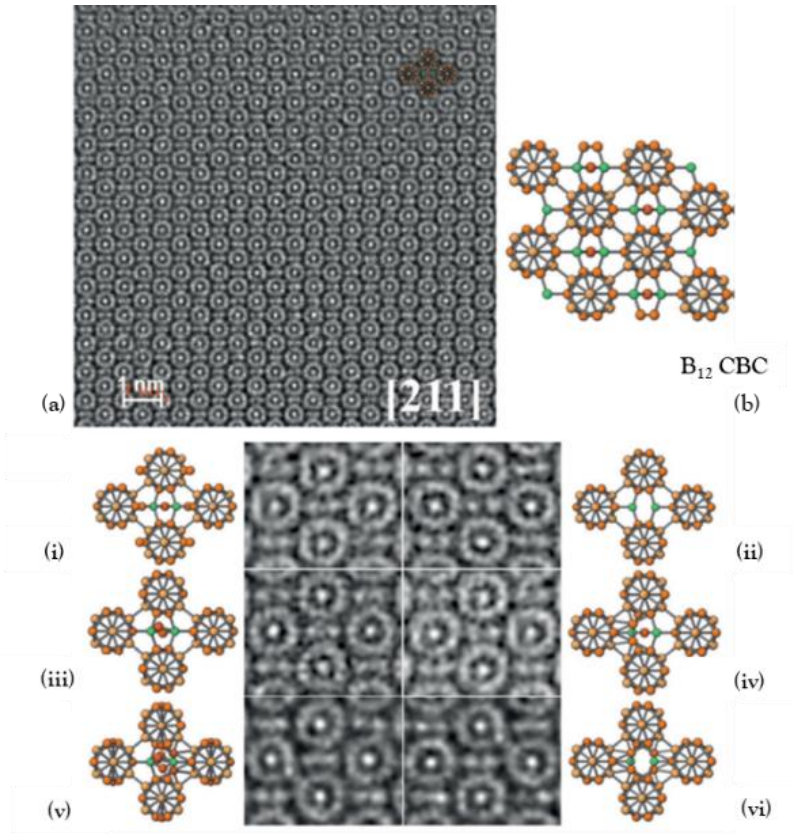


**Figure 2.8.** High resolution transmission electron microscopy of $B_{13}C_2$ along direction [211]: (a) TEM image, (b) projection of the ideal $B_{12}CBC$ structure; (i–vi) $B_{13}C_2$ chain model proposals [3].

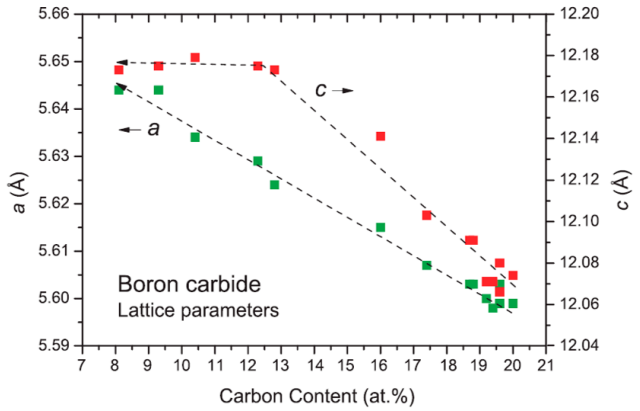


**Figure 2.9.** Boron carbide hexagonal lattice parameters [5].

## 2.2. Boron Carbide: Densification and mechanical properties

As mentioned in Chapter 1, in order for their mechanical properties to be suitable for industrial uses, $B_4C$–based materials must be fully dense and have microstructures with a grain size as fine as possible. Nonetheless, the fabrication of materials with these characteristics is a great challenge due to $B_4C$'s poor sinterability. This is conditioned by both intrinsic and extrinsic factors. First, $B_4C$'s high melting point and the low self–diffusion coefficients of B and C impose severe kinetic constraints on mass transport and hence on densification, so that full densification of these materials can only be achieved at very high temperatures. And second, $B_4C$'s oxidic impurities – in particular, passivating layers of boria ($B_2O_3$) on the $B_4C$ particle surfaces [15] – generate gas at around 1000 °C, thus favouring surface diffusion or vapour phase, and promoting grain growth over densification. It is therefore necessary to adopt strategies that can address these problems.

This subchapter will review and analyse the results of the most relevant studies on sintering $B_4C$–based materials that have been published in the recent decades. First, the studies on sintering pure $B_4C$ will be reviewed, and then $B_4C$ in the presence of other compounds that act as sintering additives or toughening second phases. The first part is organized in accordance with the sintering technique used, and the second according to the phases present in the resulting sintered composite materials. The information will be presented in tables containing the following data: number (No), product (P), starting powders (if necessary) (SP), sintering technique (ST), sintering conditions (SC), relative density (RD), hardness (H), toughness ($K_{IC}$), year (Y), and publication reference (R). The table rows will run from higher to lower relative density within each manufacturing technique used.

### 2.2.1. Sintering of pure boron carbide

Pressureless sintering of $B_4C$

Conventional sintering (pressureless sintering, PLS) is the simplest and cheapest technique existing to fabricate $B_4C$ parts (as well as any other ceramic) since it is done without simultaneous application of pressure. The powders are compacted cold prior to sintering, generally by uniaxial or isostatic pressing, giving rise to a green material with sufficient mechanical integrity to allow its manipulation. The resulting powder compacts (generally contained inside a graphite die) are loaded into a

sintering furnace for their final processing, applying the thermal cycle most appropriate for each case. In its simplest form, the selection of the thermal cycle involves choosing the heating ramp up to the maximum sintering temperature, the residence time at that temperature, and the cooling ramp. In PLS, the heat source consists of thermal resistances located inside the furnace, and are therefore at a certain distance from the material to be sintered. In this way, the compacted powder is heated by the thermal radiation emitted when the resistors are heated by the Joule effect. For this reason, conventional sintering requires very long times (10–20 hours), which have the unfortunate effect of favouring grain growth. As mentioned above, the passivation of the $B_4C$ particles also favours grain growth over densification, and this, together with the fact that the $B_4C$ is a non–oxidic ceramic and that graphite furnaces are used given the high temperatures of densification, means that the sintering has to be done in a vacuum and/or under a flow of inert gas. This, due to the lack of oxygen, not only prevents the growth of the boria layer but also serves to eliminate any boria gas that has been formed. The inert gas generally used is argon. **Table 2.3** compiles the results of different studies done to date on the fabrication of pure $B_4C$ using PLS.

**Table 2.3.** $B_4C$ pressureless sintering.

| No | P | ST | SC | RD (%) | H (GPa) | $K_{IC}$ (MPa·m$^{1/2}$) | Y | R |
|---|---|---|---|---|---|---|---|---|
| 1 | $B_4C$ | PLS | 2170°C, 15min, Ar | ~95.6 | ~24.5 | ~3.2 | 1988 | [16] |
| 2 | | | 2250°C, 120min, Ar | ~95.5 | ~21.0 | – | 2005 | [17] |
| 3 | | | 2190°C, 60min, Ar+vacuum | ~95.0 | – | – | 2004 | [18] |
| 4 | | | 2375°C, 60min, vacuum | ~93.0 | ~25.0 | – | 2006 | [19] |
| 5 | | | 2250°C, He | ~92.7 | – | – | 2003 | [20] |
| 6 | | | 1600°C–2260°C, 60min, vacuum | ~90.5 | – | – | 2019 | [21] |
| 7 | | | 2275°C, 60min, vacuum | ~86.6 | ~26.9 | | 2008 | [22] |
| 8 | | | 2150°C, vacuum | ~86.0 | ~22.0 | ~2.2 | 2008 | [23] |
| 9 | | | 2150°C, 15min, Ar | ~85.0 | – | – | 1992 | [24] |
| 10 | | | 2180°C, 120min, Ar | ~83.0 | – | – | 2007 | [25] |
| 11 | | | 2180°C, 60min, vacuum | ~83.0 | – | – | 2018 | [26] |
| 12 | | | 2250°C, 60min | ~82.5 | – | – | 2003 | [27] |
| 13 | | | 2150°C, 90min, Ar | ~81.4 | ~17.1 | ~2.6 | 2020 | [28] |
| 14 | | | 2250°C, 60min, Ar | ~79.6 | ~21.3 | ~1.8 | 2020 | [29] |
| 15 | | | 2250°C, 60min, Ar | ~79.6 | ~21.3 | ~1.8 | 2021 | [30] |
| 16 | | | 2150°C, 15min, Ar | ~78.0 | – | – | 1981 | [31] |
| 17 | | | 2050°C, 60min, inert | ~74.0 | ~18.0 | ~1.9 | 2006 | [32] |
| 18 | | | 2050°C, 60min, Ar | ~72.0 | ~19.0 | ~2.0 | 2006 | [33] |
| 19 | | | 2260°C, 15min, Ar–$N_2$ | ~71.9 | – | – | 1977 | [34] |
| 20 | | | 2190°C, 60min, Ar | ~71.0 | – | – | 2000 | [35] |
| 21 | | | 2050–2150°C, 60min, Ar | ~65.0 | ~8.5 | ~2.7 | 2010 | [36] |
| 22 | | | 2050°C–2150°C, 60min, Ar | ~64.0 | ~7.5 | ~2.7 | 2011 | [37] |

As can be seen in the table, no works were found in which fully dense (RD≥98.5%) $B_4C$ ceramics were fabricates despite using very high temperatures (over 2000 °C). Indeed, in no case did the maximum densities reach an RD of 96%. Logically, the greatest hardnesses (~25–26 GPa) correspond to the densest materials, although in no case do they reach 30 GPa (super–hard). Nonetheless, the results in **Table 2.3** show some deviations from this expectation since there are materials with similar porosities but with different hardnesses, and some materials with greater hardness than others which are less porous. The explanation lies in the fact that the hardness values obtained in the different studies depend not only on the porosity but also on other factors such as the type of hardness test used (Vickers, Knoop, *etc.*), grain size, and even the load used during the test. Indeed, the Knoop hardness values are significantly lower than the Vickers values [38], especially when it comes to ultra–hard (>20 GPa) ceramic materials such as $B_4C$ in which the difference may surpass 5 GPa. As the sintering temperature increases, the hardness should increase because of decreasing porosity, but at the same time it also should decrease because of increasing grain size. A good example of grain growth is observed in the material made with submicron (~0.8 μm) powder at 2375 °C, since the grain size of the final sintered material is 100–120 μm (**Fig. 2.10**).

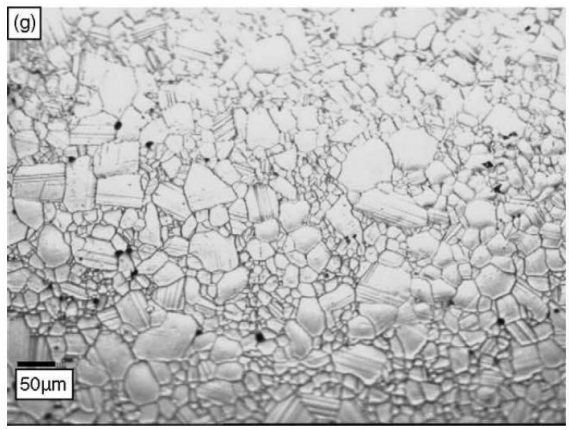


**Figure 2.10.** Microstructure of $B_4C$ sintered by PLS at 2375 °C for 60 min [19].

The hardness may be overestimated when loads of less than 10 N are used, with overestimate being worse the lesser the applied load. This is especially the case for ultra–hard materials such as $B_4C$. Finally, the use of low loads to get an estimate of the hardness of porous materials can lead to widely varying results since the values obtained will depend on whether or not there exist pores both in the tested area and

in its surroundings. In sum, hardness's dependence on porosity, type of test, grain size, and the load used greatly complicates comparison of the values reported in the different studies. **Table 2.3** also lists the toughness values of these materials. The highest value, 3.2 MPa·$m^{1/2}$, corresponds to the densest material (~95.6%). It should be noted that in some cases the toughness values in **Table 2.3** were obtained by Vickers tests [39], and that, since they are porous materials, these values would overestimates. Indeed, with this methodological approach, the greater the porosity, the greater the overestimate.

## Hot-pressing of $B_4C$

Hot-pressing (HP) is a sintering technique in which a simultaneous uniaxial pressure (30–40 MPa) is applied during heating. The only difference between PLS and HP equipment is the hydraulic press that applies a pre-set pressure during the sintering cycle. The pressure exerted favours inter-particle contact, reducing diffusion distances and promoting plastic deformation, and thereby favouring densification. It also facilitates rearrangement of the powder particles, eliminating pores and breaking up possible clumps, again favouring densification. **Table 2.4** lists the results of studies carried out in recent years on pure $B_4C$ using HP.

**Table 2.4.** $B_4C$ Hot-pressing sintering.

| No | P | ST | SC | RD (%) | H (GPa) | $K_{IC}$ (MPa·$m^{1/2}$) | Y | R |
|---|---|---|---|---|---|---|---|---|
| 1 | $B_4C$ | HP | 2202°C, 34.4MPa | ~99.6 | – | – | 1983 | [40] |
| 2 | | | 1850°C, 30MPa, 60min, $N_2$ | ~99.5 | ~21.0 | ~5.4 | 2008 | [41] |
| 3 | | | 1950°C, 30MPa, 60min, Ar | ~99.4 | ~31.0 | ~3.3 | 2020 | [7] |
| 4 | | | 1900°C, 50MPa, 60min, Ar | ~99.0 | – | ~2.5 | 2003 | [42] |
| 5 | | | 1950°C, 30MPa, 60min, vacuum+Ar | ~99.0 | – | – | 2015 | [43] |
| 6 | | | 2100°C, 25MPa, 60min, Ar | ~98.8 | ~30.8 | ~4.4 | 2016 | [44] |
| 7 | | | 2200°C, 22MPa, 10min | ~98.0 | – | – | 1979 | [45] |
| 8 | | | 2150°C, 36MPa, 60min, inert | ~95.5 | ~32.5 | ~3.0 | 2005 | [46] |
| 9 | | | 2100°C, 40MPa, 30min, Ar | >95.0 | – | – | 1989 | [47] |
| 10 | | | 2150°C, 35MPa, 65min | ~95.0 | ~29.0 | ~2.5 | 2002 | [48] |
| 11 | | | 2150°C, 35MPa, 65min, Ar | ~95.0 | ~21.0 | ~2.6 | 2009 | [49] |
| 12 | | | 1950°C, 60MPa, 60min, vacuum+Ar | ~94.5 | ~25.2 | ~3.3 | 2017 | [50] |
| 13 | | | 1950°C, 40MPa, 60min, Ar | ~92.4 | – | – | 2019 | [51] |
| 14 | | | 1950°C, 30MPa, 60min, vacuum+Ar | ~91.7 | ~24.1 | ~3.34 | 2014 | [52] |
| 15 | | | 1950°C, 30MPa, 60min, vacuum+Ar | ~90.0 | – | – | 2018 | [53] |
| 16 | | | 1900°C, 30MPa | ~83.0 | ~7.8 | ~2.1 | 2016 | [54] |
| 17 | | | 1850°C, 30MPa, 30min | ~82.3 | ~8.2 | ~2.1 | 2019 | [55] |
| 18 | | | 2050°C, 50MPa, 60min, Ar | ~79.3 | – | ~1.9 | 2003 | [56] |

Unlike the case with conventional sintering, there have been several studies in which fully dense materials were obtained at temperatures in the range ~1900–2200 °C and pressures in the range ~25–50 MPa. Therefore, the pressure exerted during heating is a key to attaining full densification of pure $B_4C$. Indeed, the greater the pressure, the lower the temperature required. As can be seen in the table, the dense materials obtained by HP are generally super–hard, with hardness values of ~30–31 GPa. Their toughness varies widely, even when the same experimental method is used. The values reported range from ~2.5 to 5.4 $MPa{\cdot}m^{1/2}$. On average, the values are clearly superior to those of PLS since the latter's products are, as mentioned above, always porous.

Hot isostating pressing of $B_4C$

In sintering by hot isostatic pressing (HIP), a much higher pressure is applied during heating than in HP (100–300 MPa *vs* 25–50 MPa), and it is applied isotropically (in all directions). Sintering temperatures are considerably reduced because this methodological approach is very effective in promoting contact between the particles, and hence the material's densification. It is a very sophisticated and costly technique, which may be why no literature could be found on the fabrication of pure $B_4C$ by HIP, although one study uses PLS followed by HIP to completely densify $B_4C$ [57], with the resulting hardness being comparable to that of the same material fabricated by HP (~27.0 GPa).

Spark–plasma sintering of $B_4C$

In spark plasma sintering (SPS), uniaxial pressure is also applied during heating, although somewhat greater than that applied in the HP technique (~50–75 MPa *vs* 25–50 MPa). Unlike the latter however, the heating in SPS is very rapid (some minutes), thus minimizing grain growth in favour of densification. **Fig. 2.11** shows the microstructure of the dense $B_4C$ made using SPS with an average 0.5 μm size starting powder. As can be appreciated, with this technique it is possible to approximately retain the initial powder particle size during densification.

To achieve ultra–fast heating, SPS equipment has two copper electrodes contacting the graphite die holding the ceramic powders. A pulsed, high intensity, low voltage electric current is run through these electrodes. The current heats the graphite die by the Joule effect, thus also heating the ceramic powder inside.

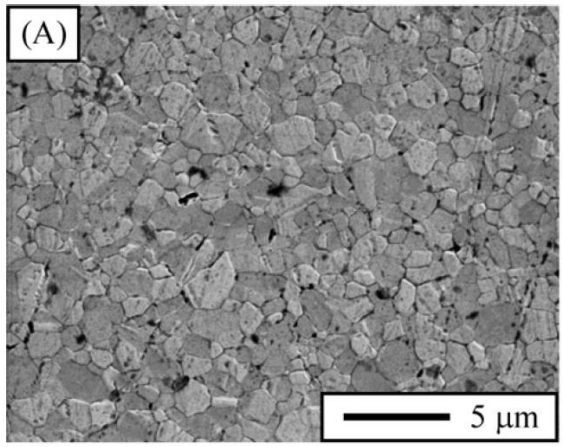


**Figure 2.11.** Microstructure of $B_4C$ sintered by SPS [8].

If the powders are themselves good electrical conductors, electrical current also flows through them. In any case, the heating of the material to be sintered is "immediate" with the passage of the current [58]. **Table 2.5** summarizes the results of the studies on fabricating pure $B_4C$ using SPS.

**Table 2.5.** $B_4C$ spark–plasma sintering.

| No | P | ST | SC | RD (%) | H (GPa) | $K_{IC}$ ($MPa \cdot m^{1/2}$) | Y | R |
|---|---|---|---|---|---|---|---|---|
| 1 | | | 1700°C, 75MPa, 3min, vacuum | ~100 | ~39.3 | ~3.5 | 2013 | [8] |
| 2 | | | 1650°C, 80MPa, 5min, vacuum | ~100 | ~34.5 | ~4.3 | 2020 | [59] |
| 3 | | | 1800°C, 50MPa, 5min, Ar | ~99.9 | ~34.0 | ~3.4 | 2019 | [60] |
| 4 | | | 1800°C, 60MPa, 13min | ~99.7 | ~33.9 | – | 2017 | [61] |
| 5 | | | 1670°C, 40MPa, vacuum | ~99.6 | ~30.7 | ~4.8 | 2015 | [62] |
| 6 | | | 1900°C, 50MPa, 25min, Ar | ~99.1 | ~37.0 | ~3.4 | 2021 | [63] |
| 7 | | | 1700°C, 75MPa, 3min, vacuum | ~99.1 | – | – | 2015 | [64] |
| 8 | | | 1800°C, 50MPa, 5min, vacuum | ~99.0 | ~39.1 | ~5.3 | 2010 | [65] |
| 9 | | | 2100°C, 40MPa, 20min, vacuum+$N_2$ | ~99.0 | – | – | 2018 | [66] |
| 10 | $B_4C$ | SPS | 1700°C, 75MPa, 3min, vacuum | ~98.8 | ~37.0 | ~2.9 | 2014 | [67] |
| 11 | | | 1650°C, 100MPa, 5min, vacuum | ~98.0 | ~42.6 | ~2.6 | 2017 | [68] |
| 12 | | | 1500°C, 75MPa, 3min, vacuum | ~98.0 | ~34.2 | ~3.0 | 2016 | [69] |
| 13 | | | 1700°C, 45MPa, 10min, Ar | ~95.8 | ~38.1 | ~3.2 | 2017 | [70] |
| 14 | | | 1800°C, 50MPa, 5min | ~95.4 | ~36.6 | ~2.1 | 2014 | [71] |
| 15 | | | 1800°C, 75MPa, 3min, vacuum | >95.0 | ~29.0 | – | 2018 | [72] |
| 16 | | | 1800°C, 50MPa, 10min | ~94.3 | ~35.6 | ~2.4 | 2020 | [73] |
| 17 | | | 1800°C, 75MPa, 3min | ~91.3 | – | – | 2021 | [74] |
| 18 | | | 1700°C, 50MPa, 5min, vacuum | ~90.4 | ~28.1 | ~3.4 | 2014 | [75] |
| 19 | | | 1700°C, 32MPa, 5min | ~84.5 | ~17.9 | ~2.9 | 2016 | [76] |
| 20 | | | 1800°C, 35MPa, 6min, vacuum | ~77.0 | – | – | 2014 | [77] |

As can be appreciated, the sintering temperatures necessary to obtain dense materials are reduced by some 100–200 °C relative to HP, depending on the pressure applied. In addition, materials with hardnesses in the range of ~30–40 GPa are obtained, in some cases much greater than the hardnesses of materials fabricated using HP (~30 GPa). This is because, as mentioned above, the ultra–fast heating allows the initial particle size to be retained, so that it is possible to fabricate materials with different grain sizes (nanometric, submicron, or micron) and, therefore, with different hardnesses. The toughness values (~3.5–5 $MPa \cdot m^{1/2}$) seem greater than those of dense materials fabricated by HP. The resulting values also present lower variability.

Flash sintering of $B_4C$

Flash Sintering (FS), like the SPS technique, is also ultra–fast, but does not apply pressure. The technique is based on the "flash effect" of an abrupt rise in conductivity under certain conditions of temperature and applied electric field. The flash event only occurs above a certain value of the electric field (several tens of V/cm), and depends on the material. It is usually accompanied by a flash with dissipation of energy (Joule effect) in the range of 10–50 $mW/mm^3$ [78]. This technique generates faster heating than SPS, and materials can be fabricated in a matter of seconds or minutes without the need to apply simultaneous pressure. It would thus be expected that materials can be fabricated with properties similar to or better than those obtained by SPS. Nonetheless, it is thought that, given their fabrication conditions, these are materials that have not reached equilibrium. The difference between FS and SPS is in the form of heating, since in FS it is not the graphite die that conducts most of the electrical current but the sample itself. Only one study could be found in which $B_4C$ was fabricated using FS [79]. It resulted in uneven densification, with some zones in the material of ~99.5% RD and others of ~89% RD.

In summary, the studies carried out to date on the fabrication of $B_4C$ clearly indicate the impossibility of obtaining fully dense materials by conventional sintering, and that the simultaneous application of pressure during heating is required (as in the cases of the advanced pressure sintering techniques, HP and SPS). With the HP technique, fully dense $B_4C$ can be fabricated at temperatures ≥1900 °C and pressures of ~25–50 MPa. Logically, the lower the applied pressure, the higher the temperature

required to achieve full densification. The SPS technique reduces manufacturing temperatures by approximately 100–200 °C, so that fully dense $B_4C$ can be fabricated at temperatures ≥1700 °C and at pressures of ~50–75 MPa. This reduction in temperature is in fact not totally real since the temperature recorded by the optical pyrometers during SPS is not that of the $B_4C$ powder but that of the graphite matrix, which is cooler. The SPS technique is not any more sophisticated than that of HP, but, being ultra–fast, it offers two major advantages over the latter. One is that the lower temperatures and shorter times allow manufacturing that is both more profitable (by reducing energy consumption costs) and more respectful with the environment. The other is that it allows dense materials of different grain sizes and therefore optimized hardness to be fabricated.

### 2.2.2. Boron carbide sintering with additives

In addition to applying pressure and/or reducing sintering time using ultra–fast techniques, other compounds can be mixed in to facilitate $B_4C$'s sintering. These additives may or may not be in the solid state. If, once sintered, second–phase residuals remain, then what is actually obtained is a composite $B_4C$–based material, even though the proportion of the second phases may be minor. As is logical, the presence of these phases also influences the mechanical properties of the final material. The ideal therefore is to choose additives which, in addition to promoting the $B_4C$'s sintering, generate secondary phases that are light, refractory, and with hardnesses that are as close as possible to $B_4C$'s.

The list of additives that have been used to densify $B_4C$ is long. Furthermore, the additive itself is less relevant than the composition of the final material, since the additives generally react with the $B_4C$, being partially or totally consumed to give rise to other products. The organization of this part of the literature review will therefore be in accordance with the nature and number of the phases appearing in the final composites rather than with the additives themselves – firstly, whether the final composite has minority soft phases based on carbon (graphite, graphene oxide, carbon nanotubes, *etc.*), and secondly, whether the final composite contains other minor ceramic phases of high hardness (carbides, borides, nitrides, and oxides) and, occasionally, also other carbonaceous phases. In both cases, proportions of additives necessary to facilitate sintering are used that, if possible, augment the material's toughness, to some extent alleviating the main drawback of using $B_4C$ in structural applications, but without excessively compromising its hardness.

## Boron carbide with carbonaceous phases

Carbon was one of the first additives used in conventional sintering. Its effectiveness is based on the fact that it allows $B_2O_3$ impurities to be eliminated in accordance with the reaction:

$$2B_2O_3+7C \rightarrow B_4C+6CO(g) \quad (2.1)$$

and therefore reduces grain growth in favour of densification. The removal of the oxide layer facilitates direct contact between the $B_4C$ particles, so that sintering starts at relatively low temperatures (~1350 °C). Furthermore, since there is no vapour phase, mass transport is promoted by diffusion across the grain boundary or through the crystal lattice. Various studies have applied different types of carbon (graphite, phenolic resin, *etc.*) as an additive in conventional $B_4C$ sintering. Nonetheless, although the relative densities of these materials are greater than in the absence of carbon, none of them reached full densification. This is not the case when the additives are carbonaceous reinforcements in the form of tubes, fibres, platelets, *etc.* since they yield full densification of the $B_4C$–based composite while preserving its lightness and providing toughness reinforcement mechanisms (crack bridging, crack deflection, *etc.*). However, the main problem to resolve is to disperse these additives evenly in the $B_4C$ matrix. Generally, nanocarbon reinforcements, the commonest today in brittle ceramics, are classified into zero–dimensional (carbon nanoparticles, CNPs), one–dimensional (carbon nanotubes, CNTs), and two–dimensional (graphene platelets, GPL; graphene nanoplates GNPs; reduced graphene oxide, rGO; *etc.*). CNPs provide optimal lubrication for wear applications but are not very effective in increasing toughness. CNTs provide greater toughness, although they are difficult to disperse in the $B_4C$ matrix since they are elongated and tend to roll up and agglomerate. They are also more costly to produce. The two–dimensional nanocarbon reinforcements are those with the greatest potential for improving toughness (due to the dimensionality of the cracks), and they are more easily dispersed in the ceramic matrix. **Table 2.6** lists the results of studies on fabricating carbon reinforced $B_4C$ using HP and SPS.

As can be seen, HP yields dense materials at 1950–2100 °C and 25–30 MPa, and SPS at 1620–1800 °C and 40–50 MPa. In both cases, the materials obtained exhibit a good combination of mechanical properties, with hardness somewhat greater than 30 GPa and toughness of about 5 $MPa \cdot m^{1/2}$. Comparison of these results with those of **Tables 2.4** and **2.5** corresponding to $B_4C$ materials fabricated by

**Table 2.6.** Sintering of the $B_4C$ with nanocarbon reinforcements.

| No | P | SP | ST | SC | RD (%) | H (GPa) | $K_{IC}$ ($MPa \cdot m^{1/2}$) | Y | R |
|---|---|---|---|---|---|---|---|---|---|
| 1 | $B_4C$–2wt.%rGO | $B_4C$+GO# | HP | 1950°C, 30MPa, 60min, Ar | ~99.9 | ~33.0 | ~5.9 | 2020 | [7] |
| 2 | $B_4C$–1wt.% GNPs | $B_4C$+GNPs | | 1950°C, 30MPa, 60min, vacuum+Ar | ~99.1 | ~32.8 | ~4.7 | 2020 | [80] |
| 3 | $B_4C$–GPL | $B_4C$+4.5 wt.% GPL | | 2100°C, 25MPa, 60min, Ar | AFD* | ~30.4 | ~5.9 | 2016 | [81] |
| 4 | $B_4C$–2.0vol.% rGO | $B_4C$+GO | SPS | 1800°C, 50MPa, 5min, Ar | ~99.7 | ~32.8 | ~4.9 | 2019 | [60] |
| 5 | $B_4C$–CNT | $B_4C$+0.5 wt.% CNT | | 1620°C, 40MPa, vacuum | ~99.5 | ~32.2 | ~5.2 | 2015 | [62] |

#Graphene oxide * Almost fully dense

HP and SPS without nanocarbon reinforcements suggests that, in the presence of these toughening phases, *(i)* it is possible to reduce the sintering temperature of $B_4C$ moderately, *(ii)* the hardness penalty is irrelevant since the materials obtained are also super–hard, and *(iii)* the toughness is significantly improved.

### $B_4C$ materials with ceramic second phases

Next, the studies of fabricating $B_4C$ with other ceramic phases will be reviewed, starting with those that use only one additional phase, then two, and finally three or more.

### Two–phase $B_4C$–based compounds

There has been work on the fabrication of two–phase $B_4C$–based compounds with transition metal diborides as minor phases (**Table 2.7**). As one sees in the table, these are $TiB_2$ and $ZrB_2$ (both group IV), $TaB_2$ (group V), and $CrB_2$ (group VI). They exhibit a good combination of properties.

**Table 2.7.** Properties of $B_4C$ and some metalic diborides.

| Properties | $B_4C$ | $TiB_2$ [83] | $ZrB_2$ [83] | $TaB_2$ [83] | $CrB_2$ [83] |
|---|---|---|---|---|---|
| Density ($g/cm^3$) | ~2.52 [2] | ~4.53 | ~6.09 | ~12.62 | ~5.6 |
| Melting point (°C) | ~2490 [10] | ~3063 | ~3473 | ~3310 | ~2473 |
| Hardness (GPa) | ~31[7]-39[8] | ~33 | ~22.1 | ~24.5 | ~20.6 |
| Toughness ($MPa{\cdot}m^{1/2}$) | ~2 [82] | ~6-8 [84] | ~2.3-3.5 [85] | ~4-5 [86] | ~3-4 [87] |
| Thermal expansion coefficient ($\times10^{-6}{\cdot}K^{-1}$) | ~6.5 [8] | ~8.6 | ~8.3 | ~8.4 | ~10.5 [87] |

*The $B_4C$–$TiB_2$ system*

Compared with the rest of the above diborides, $TiB_2$ is the one that has properties closest to those of $B_4C$, and this probably is the reason why more studies were found with a focus on fabricating the $B_4C$–$TiB_2$ system **(Table 2.8)** than the $B_4C$–$ZrB_2$, $B_4C$–$TaB_2$, or $B_4C$–$CrB_2$ systems.

**Table 2.8.** Sintering of the $B_4C$–$TiB_2$ two-phase system.

| No | P | SP | ST | SC | RD (%) | H (GPa) | $K_{IC}$ ($MPa{\cdot}m^{1/2}$) | Y | R |
|---|---|---|---|---|---|---|---|---|---|
| 1 | $B_4C$–$TiB_2$ | $B_4C$+ 15wt.% $TiO_2$+ 1-6wt.%C | PLS | 1900-2050°C, 60min, Ar | >99.0 | - | ~3.7 | 1996 | [88] |
| 2 | $B_4C$–$TiB_2$ | $B_4C$+ 30wt.%$TiB_2$ | | 2150°C, vacuum | ~98.5 | ~23.0 | ~3.4 | 2008 | [23] |
| 3 | $B_4C$- 30vol.% $TiB_2$ | $B_4C$+$TiB_2$ | HP | 2000°C, 35MPa, 60min, vacuum | ~100 | ~30.4 | ~5.2 | 2018 | [89] |
| 4 | $B_4C$–$TiB_2$ | $B_4C$+$TiO_2$+C | | 2000°C, 50MPa, 60min | ~100 | - | ~3.0 | 2005 | [90] |
| 5 | $B_4C$- 30vol.% $TiB_2$ | $B_4C$+$TiO_2$+ carbon black | SPS | 2000°C, 60MPa, 5min, vacuum | ~100 | ~39.3 | ~3.0 | 2011 | [91] |
| 6 | $B_4C$–$TiB_2$ | $B_4C$+ 30wt.%$TiO_2$ | | 1900°C, 50MPa, 30min | ~100 | ~35.0 | - | 2018 | [92] |
| 7 | $B_4C$- 5vol.% $TiB_2$ | $B_4C$+$TiO_2$ | | 2100°C, 35MPa, 10min, vacuum | ~99.2 | ~30.7 | ~3.3 | 2020 | [93] |

The additives used to obtain this secondary phase are $TiB_2$ directly or $TiO_2$, the latter because it reacts with $B_4C$ giving rise to $TiB_2$ in accordance with the following reactions corresponding to the absence and the presence of carbon, respectively:

$$5B_4C+6TiO_2 \rightarrow 6TiB_2+4B_2O_3+5C \quad (2.2)$$

$$B_4C+2TiO_2+3C \rightarrow 2TiB_2+4CO(g) \quad (2.3)$$

In the second case, the reaction takes place without forming boria, although this phase is always present, passivating the $B_4C$ particles. Nonetheless, as noted above, the boria can be partially or totally eliminated with an excess of carbon present as an impurity in the $B_4C$ starting powders, added intentionally as a sintering additive and/or present as an impurity in the $B_4C$ starting powder. Finally, the graphite die can cause carbon contamination during sintering, especially in HP and SPS because of the direct contact. Regardless of the origin of the C, its presence during sintering plays a fundamental role in promoting densification.

When $TiO_2$ is used as a sintering additive, in principle its melting point of ~1843 °C [94] would allow accelerated densification of the material, especially in comparison with the solid–state sintering that takes place when using $TiB_2$. This is because the liquid would quickly fill the pores in the material. It is important to emphasize that the liquid–phase is transitory and disappears by reacting with $B_4C$ and/or C giving rise to $TiB_2$, whose melting point is much higher. Generally, liquid–phase densification favours grain refinement during sintering (since the sintering temperatures are much lower). It is therefore to be expected that the hardness of these materials will be greater than that of materials fabricated with $TiB_2$ additives directly. Indeed, the greatest hardness values in **Table 2.8** correspond to $TiO_2$ additives. Therefore, the selection of additives that generate a liquid–phase at temperatures below that of the fabrication conditions seems quite appropriate. Also, by fully reacting with $B_4C$, these additives disappear to form refractory compounds, thus avoiding the compromise that their presence in the final composite would otherwise entail for high temperature applications.

The toughness values are moderate (~3 $MPa \cdot m^{1/2}$) except for one specific study. The main mechanism of toughness reinforcement observed in these materials is crack deflection. A crack passes through the $B_4C$ grains (transgranular fracture), but tends to go around the $TiB_2$ grains (intergranular fracture) because the thermal expansion coefficient of $TiB_2$ is greater than that of $B_4C$, so that, unlike the case of pure $B_4C$, the trajectory of the crack is not linear. Being more tortuous, the crack

requires more energy to propagate, making the composite material somewhat tougher.

*The $B_4C$–$ZrB_2$ system*

The next diboride presenting the best combination of properties is $ZrB_2$, being the most refractory of all the group. **Table 2.9** lists the studies corresponding to the $B_4C$–$ZrB_2$ two–phase system. As can be seen, unlike the case with $TiB_2$, no studies were found that used $ZrB_2$ starting powders, probably because it is highly refractory. The commonest form of obtaining $ZrB_2$ is through the following reactions corresponding to the absence or presence of additional carbon, respectively:

$$2ZrO_2+B_4C \rightarrow 2ZrB_2+B_2O_3+CO(g) \quad (2.4)$$

$$2ZrO_2+B_4C+3C \rightarrow 2ZrB_2+4CO(g) \quad (2.5)$$

**Table 2.9.** Sintering of the $B_4C$–$ZrB_2$ two–phase system.

| No | P | SP | ST | SC | RD (%) | H (GPa) | $K_{IC}$ ($MPa{\cdot}m^{1/2}$) | Y | R |
|---|---|---|---|---|---|---|---|---|---|
| 1 | $B_4C$–$ZrB_2$ | $B_4C$+ 15wt.% $ZrO_2$ | HP | 1950°C, 30MPa, 60min, vacuum+Ar | ~99.3 | – | – | 2018 | [53] |
| 2 | $B_4C$–30vol.% $ZrB_2$ | $B_4C+ZrO_2$+ carbon black | SPS | 2000°C, 30MPa, 5min, vacuum | FD* | ~30.6 | ~3.0 | 2014 | [95] |
| 3 | $B_4C$–$ZrB_2$ | $B_4C$+ 10wt.% $ZrH_2$ | SPS | 1700°C, 32MPa, 10min, vacuum | ~98.8 | ~31.3 | ~4.2 | 2015 | [96] |

Another form of obtaining $B_4C$–$ZrB_2$ composites is through reactive sintering of a $B_4C+ZrH_2$ powder mixture, in accordance with the following reaction:

$$B_4C+2ZrH_2 \rightarrow 2ZrB_2+C+2H_2(g) \quad (2.6)$$

Unlike $ZrO_2$, $ZrH_2$ is not refractory since it melts at ~800 °C [97], and favours sintering with a transient liquid–phase which therefore promotes the production of dense materials even at relatively low temperatures. As in the case when using $TiO_2$, the C product resulting from the reaction helps to remove $B_2O_3$ impurities.

Comparatively, it can be seen that the choice of $ZrB_2$ instead of $TiB_2$ reduces the hardness of the final composite materials moderately, although both cases are super–hard with hardnesses greater than 30 GPa. These composite materials' toughness is similar to that of the previous two–phase system because they have the same toughness reinforcement mechanism (crack deflection).

*The $B_4C$–$CrB_2$ and $B_4C$–$TaB_2$ systems*

Only one study was found for each of these two biphasic systems (**Table 2.10**). That for the $B_4C$–$CrB_2$ system was carried out directly using $CrB_2$ powders as the secondary phase, whose melting point (2473 °C) is very high and similar to that of $B_4C$. Therefore, the densification of these composites at 1900 °C must be by solid–state sintering. Of all the borides listed in **Table 2.7**, $CrB_2$ is the softest (with a hardness of 20.6 GPa), although the hardness of the composite was not given. Its toughness, however, was indicated to be moderate.

**Table 2.10.** Sintering of the $B_4C$–$CrB_2$ and $B_4C$–$TaB_2$ two–phase systems.

| No | P | SP | ST | SC | RD (%) | H (GPa) | $K_{IC}$ (MPa·m$^{1/2}$) | Y | R |
|---|---|---|---|---|---|---|---|---|---|
| 1 | $B_4C$–$CrB_2$ | $B_4C$+ 13vol.%$CrB_2$ | HP | 1900°C, 50MPa, 60min, Ar | ~99.0 | – | ~3.5 | 2003 | [42] |
| 2 | $B_4C$–$TaB_2$ | $B_4C$+ 33mol%$TaB_2$ | SPS | 2350°C, 60MPa, 1min, Ar | ~99.8 | ~26.0 | ~4.5 | 2016 | [98] |

The $B_4C$–$TaB_2$ system study showed this composite to be softer than the previous two–phase systems, but to have much more optimized toughness. As can be seen in **Table 2.7**, $TaB_2$ is, together with $ZrB_2$, one of the most refractory diborides (its melting point is 3310 °C), and it has great chemical stability, which is why the $B_4C$–$TaB_2$ two–phase system might be very interesting for the fabrication of cutting tools, among other applications. Nonetheless, very high temperatures are needed to fabricate these composites, and they are heavy (density 5.0 g/cm$^3$), and considerably penalize the characteristic hardness of dense $B_4C$ (≥30 GPa).

*The $B_4C$–$SiC$ system*

In addition to diborides, metal carbides are also excellent candidates for incorporation as secondary phases in $B_4C$ matrices. SiC particularly stands out because its properties are the closest to $B_4C$ (its density is ~3.2 g/cm$^3$ and its melting point is ~2650–2950 °C, although its hardness is appreciably lower (~23–25 GPa)). In addition, it offers good wear resistance and its fracture toughness (~4.6 MPa·m$^{1/2}$) [6] is greater than that of $B_4C$. Furthermore, SiC could provide $B_4C$ composites with greater resistance to oxidation, as it already does in ultra–high temperature ceramics. This is because SiC oxidizes to form passivating protective layers of $SiO_2$, and the $SiO_2$ can react with $B_2O_3$ to form borosilicate layers. **Table 2.11** lists some of the

work on the $B_4C$–SiC system.

**Table 2.11.** Sintering of the $B_4C$–SiC two-phase system.

| No | P | SP | ST | SC | RD (%) | H (GPa) | $K_{IC}$ (MPa·m$^{1/2}$) | Y | R |
|---|---|---|---|---|---|---|---|---|---|
| 1 | $B_4C$–30wt.% SiC | $B_4C$+30wt.%α–SiC | HP | 2000°C, 40MPa, 60min, vacuum | ~99.8 | ~30.5 | ~3.6 | 2020 | [99] |
| 2 | $B_4C$–20wt.% SiC | $B_4C$+Si+C | | 1950°C, 30MPa, 60min, vacuum+Ar | ~98.6 | ~34.3 | ~6.0 | 2014 | [100] |
| 3 | $B_4C$–SiC–(Si)* | $B_4C$+8wt.%Si | SPS | 1800°C, 50MPa, 5min, vacuum | ~99.8 | ~41.8 | ~6.1 | 2010 | [65] |
| 4 | $B_4C$–SiC | $B_4C$+8wt.%Si | | 1700°C, 60MPa, 7min, vacuum | ~99.7 | ~36.7 | – | 2015 | [101] |
| 5 | $B_4C$–SiC | $B_4C$+15wt.% β–SiC | | 1700°C, 75MPa, 3min | ~99.4 | – | – | 2016 | [102] |
| 6 | $B_4C$–SiC | $B_4C$+15wt.% β–SiC | | 1700°C, 75MPa, 3min, vacuum | ~99.4 | ~36.2 | ~5.7 | 2013 | [8] |
| 7 | $B_4C$–SiC | $B_4C$+20wt.% (Si+C) | | 1800°C, 30MPa, 5min, Ar | ~99.2 | ~35.8 | ~6.8 | 2017 | [103] |
| 8 | $B_4C$–SiC–(C)* | 50wt.%$B_4C$ +SiC+ 1.5wt.%C | | 1950°C, 50MPa, 5min, vacuum | ~98.9 | ~30.3 | ~2.6 | 2021 | [104] |

*The amount of the secondary phases in parenthesis is very small

Both $B_4C$ and SiC are non-oxidic ceramics, and their particles are therefore covered with a passivating oxide layer ($B_2O_3$ and $SiO_2$, respectively). As mentioned above, this promotes grain growth to the detriment of densification. The idea therefore is that a small amount of C should be added to the powder mixture to remove the oxides. Nonetheless, this seems less critical than in the case of pure $B_4C$ because the $B_2O_3$ and $SiO_2$ can react to form a borosilicate, minimizing the problem attributable to the formation of gaseous boria at high temperatures. As can be seen in **Table 2.11**, the additives used to obtain these composites are Si and SiC, but

generally in the presence of a certain amount of free C. Obviously this will be greater if more C is added intentionally. The fundamental difference between these two additives is that with Si a liquid–phase is generated since Si melts at ~1410 °C, and this liquid then reacts with the free C and is completely consumed, producing SiC. One would expect that the densification of $B_4C$ with SiC would also occur by sintering with a liquid–phase (of borosilicates formed from the native oxides).

The hardnesses of the composite materials corresponding to the $B_4C$–SiC system are in the range of ~30–40 GPa, being greater the lower the proportion of SiC in the final composite. The results also suggest that the presence of SiC as a minor secondary phase reinforces toughness much more than in the case of metal diborides since values as high as ~6 $MPa{\cdot}m^{1/2}$ can be reached (but as long as the SiC proportion does not exceed 20 wt.%). This is because SiC has a lower thermal expansion coefficient ($4.5\times10^{-6}{\cdot}K^{-1}$) [8] than $B_4C$ ($6.5\times10^{-6}{\cdot}K^{-1}$), so that the SiC particles are subjected to compressive, rather than tensile, residual stresses, and are thus more effective in improving the toughness of the composite material.

*The $B_4C$–$Y_3Al_5O_{12}$ system*

This is the two–phase system with the least refractory and lowest hardness secondary phase of all those mentioned so far. $Y_3Al_5O_{12}$ (YAG) is the intermediate compound that corresponds to a eutectic in the $Y_2O_3$–$Al_2O_3$ phase diagram (molar ratio 3–5), with the following characteristics: melting point ~1900 °C, density ~4.56 $g/cm^3$, thermal expansion coefficient $\sim8\times10^{-6}{\cdot}K^{-1}$, and hardness ~15 GPa [105]. **Table 2.12** presents the results of the only study found for this system. It seems that densification originates by sintering with a liquid–phase, but in this case, and unlike the previous two–phase systems, it is permanent, so that the refractoriness of the composite material is limited by the secondary phase. As can be seen, the sintering temperature is moderate, but the hardness is also moderate (<30 GPa). Nonetheless, the toughness of this composite material is close to 6 $MPa{\cdot}m^{1/2}$, which is considerably greater than that of monolithic $B_4C$ ceramics and $B_4C$ composites with metal diboride secondary phases.

**Table 2.12.** Sintering of the $B_4C$–$Y_3Al_5O_{12}$ two–phase system.

| No | P | SP | ST | SC | RD (%) | H (GPa) | $K_{IC}$ ($MPa{\cdot}m^{1/2}$) | Y | R |
|---|---|---|---|---|---|---|---|---|---|
| 1 | $B_4C$–$Y_3Al_5O_{12}$ | $B_4C$+ 4wt.%$Al_2O_3$+ 6wt.%$Y_2O_3$ | HP | 1800°C, 35MPa, 60min, vacuum+Ar | ~99.8 | ~28.3 | ~5.6 | 2015 | [106] |

*The $B_4C$–hBN system*

The last two–phase $B_4C$–based system found in the literature is one that contains hexagonal boron nitride (hBN) as the secondary phase ($B_4C$–hBN). **Table 2.13** summarizes the results of a recent study on this system. Cubic BN (cBN) was used as starting powder because it is easier to disperse, and during densification it is transformed into hBN at ~1550–1625 °C. The sintering temperature seems moderate considering that BN is highly refractory. Nonetheless, the authors suggest that the exothermic transformation from cubic to hexagonal phase that occurs during sintering could facilitate densification. The resulting composite has high hardness, although its toughness is less than that of other two–phase systems such as $B_4C$–SiC. Furthermore, it seems that the toughening of the $B_4C$ attained with hBN platelets is clearly inferior to that attained with nanocarbon. However, the use of GPL is more limited since they can react with $B_4C$ and their structural stability is compromised at high temperatures [5], especially if the sintering technique used is not ultra–fast.

**Table 2.13.** Sintering of the $B_4C$–hBN two–phase system.

| No | P | SP | ST | SC | RD (%) | H (GPa) | $K_{IC}$ (MPa·m$^{1/2}$) | Y | R |
|---|---|---|---|---|---|---|---|---|---|
| 1 | $B_4C$–hBN | $B_4C$+ 5vol.%cBN | SPS | 1800°C, 50MPa, 10min | ~99.7 | ~30.5 | ~3.8 | 2020 | [73] |

## Three–phase $B_4C$–based compounds

In addition to the aforementioned two–phase composites, other three–phase materials have been fabricated with $B_4C$ as the primary phase in order to facilitate its densification, maintain its hardness, and, if possible, improve its toughness. There are multiple combinations of secondary phases in three–phase systems, since they can include borides, carbides, nitrides, *etc.* As noted above, the most widely studied two–phase systems are those with $TiB_2$ or SiC as secondary phase, since both cases yield materials that are dense and ultra–hard (hardness >30 GPa), although SiC allows much greater improvements in toughness. Therefore, first the three–phase systems in which these two compounds are the secondary phases will be discussed, and then other combinations.

*The $B_4C$–SiC–$TiB_2$ system*

**Table 2.14** lists the results of studies corresponding to the $B_4C$–SiC–$TiB_2$

system, *i.e.*, containing a carbide and a boride as minority phases. To produce materials of this type, it is necessary to use starting powders that provide Si and Ti. As indicated in the table, this has been achieved with various sintering additives: Ti–Si alloy (76 wt.% Si), $TiSi_2$, TiC+Si, $Ti_3SiC_2$, $Ti_3SiC_2$+Si, and $TiB_2$+SiC.

**Table 2.14.** Sintering of the $B_4C$–SiC–$TiB_2$ three–phase system.

| No | P | SP | ST | SC | RD (%) | H (GPa) | $K_{IC}$ ($MPa{\cdot}m^{1/2}$) | Y | R |
|---|---|---|---|---|---|---|---|---|---|
| 1 | $B_4C$–20wt.%(SiC–$TiB_2$) | $B_4C$+TiC+Si | HP | 1950°C, 60MPa, 60min, Ar | ~99.4 | ~35.2 | ~6.4 | 2019 | [107] |
| 2 | $B_4C$–SiC–$TiB_2$ | $B_4C$+10wt.%$Ti_3SiC_2$ | | 2100°C, 25MPa, 60min, Ar | ~99.6 | ~31.6 | ~7.0 | 2016 | [44] |
| 3 | $B_4C$–SiC–$TiB_2$ | 60vol.%$B_4C$+30vol.%$TiB_2$+10vol.%SiC | | 1950°C, 30MPa, 60min, vacuum+Ar | ~99.2 | ~32.8 | ~8.2 | 2018 | [108] |
| 4 | $B_4C$–10wt.%(SiC–$TiB_2$) | $B_4C$+(TiC+Si) | | 1950°C, 60MPa, 60min, vacuum+Ar | ~98.9 | ~35.5 | ~6.0 | 2017 | [50] |
| 5 | $B_4C$–SiC–$TiB_2$ | $B_4C$+30wt.%Ti–Si | | 1850°C, 30MPa, 30min | ~98.9 | ~28.4 | ~6.3 | 2019 | [55] |
| 6 | $B_4C$–SiC–$TiB_2$ | $B_4C$+16wt.%$TiSi_2$ | SPS | 1800°C, 40MPa, 5min, vacuum | ~99.2 | ~33.5 | ~6.4 | 2021 | [109] |
| 7 | $B_4C$–SiC –$TiB_2$ | $B_4C$+5wt.%($Ti_3SiC_2$+Si) | | 1700°C, 80MPa, 5min, vacuum | ~99.0 | ~38.4 | ~5.6 | 2019 | [110] |
| 8 | $B_4C$–30wt.%(SiC–$TiB_2$) | $B_4C$+$Ti_3SiC_2$+Si | | 1650°C, 80MPa, 5min | ~98.6 | ~28.5 | ~5.8 | 2018 | [111] |

The composition selected for the Ti–Si alloy is eutectic, so that it melts at ~1330 °C giving rise to a transient liquid–phase that reacts with the $B_4C$, thus disappearing to form SiC and $TiB_2$. The same is the case when using $TiSi_2$ or pure Si,

although their liquid–phases are formed at ~1410 °C and 1480 °C, respectively [112]. When only $Ti_3SiC_2$ (a MAX phase[1]) is used, densification takes place by solid–state sintering. In the case of directly incorporating both SiC and $TiB_2$ into the starting powder mixture, it has been suggested that the densification is assisted by the liquid–phase, in this case associated with the formation of oxides during the previous stage of grinding the powder mixtures. The results of **Table 2.14** indicate that in almost all cases super–hard materials with highly optimized toughness are obtained, with values as high as those obtained in the $B_4C$–SiC system which, in turn, are clearly higher than those of the $B_4C$–$TiB_2$ system. The residual stresses generated in three–phase systems are greater than in two–phase systems due to the greater number of phases with different coefficients of thermal expansion, so it would be expected that the added toughening would be similar or even greater.

### Other three–phase $B_4C$–based compounds

**Table 2.15** lists some results of recent studies on $B_4C$–based composites with SiC or $TiB_2$ and another secondary phase. There is only one study on fabricating $B_4C$ with SiC and another minor secondary phase (metal diboride), and this secondary phase was obtained from a metal disilicide, $MoSi_2$, as sintering additive. The following reaction was proposed:

$$B_4C+2MoSi_2+3C\rightarrow 4SiC+2MoB_2 \quad (2.7)$$

However, when $TiSi_2$ is used as sintering additive, the overall reaction actually occurring has been identified as being through the following two concatenated sub–reactions:

$$B_4C+2TiSi_2\rightarrow SiC+2TiB_2+3Si \quad (2.8)$$

$$3Si(l)+3C\rightarrow 3SiC \quad (2.9)$$

Thus, everything seems to indicate that when disilicides are used as additives, a transient liquid–phase (in this case Si) is generated during sintering that facilitates densification, giving rise to a final three–phase composite, with a carbide and a boride as minority secondary phases. In these cases, super–hard materials with improved toughness are obtained, evidence for the interest of using metal disilicides as sintering additives. Despite the promising results obtained with the combination

[1] MAX phases are layered hexagonal carbides and nitrides with the general formula $M_{n+1}AX_n$, where n = 1 to 3, and M is an early transition series metal, A is an element of group A (mainly IIIA and IVA, or groups 13 and 14), and X is carbon and/or nitrogen [113].

of $B_4C$ and disilicides, it is surprising to note that there have as yet been few studies on fabricating this type of three–phase composite.

**Table 2.15.** Sintering of other three–phase $B_4C$–based compounds.

| No | P | SP | ST | SC | RD (%) | H (GPa) | $K_{IC}$ (MPa·$m^{1/2}$) | Y | R |
|---|---|---|---|---|---|---|---|---|---|
| 1 | $B_4C$–SiC–$MoB_2$ | $B_4C$+30wt.%. $MoSi_2$ | HP | 1900°C, 50MPa, 120min, vacuum | ~99.2 | ~35.1 | ~4.8 | 2014 | [114] |
| 2 | $B_4C$–$TiB_2$–$W_2B_5$ | $B_4C$+30% (W,Ti)C | | 1850°C, 35MPa, 40min, Ar | ~99.2 | ~26.0 | ~3.9 | 2002 | [48] |
| 3 | $B_4C$–$TiB_2$–$Al_2O_3$ | 85.3wt.% $B_4C$+ 4.7wt.% TiC+ 10wt.% $Al_2O_3$ | | 1900–1950°C, 45–60 min | FD* | ~26.3 | ~4.0 | 2016 | [115] |
| 4 | $B_4C$–$TiB_2$–$Al_4C_3$ | $B_4C$+ 5wt.%Ti–Al | SPS | 1700°C, 32MPa, 5min | ~99.5 | ~33.5 | ~5.5 | 2016 | [76] |

*Fully dense

With respect to three–phase $B_4C$–based materials with $TiB_2$ but not with SiC, **Table 2.15** also presents the results of studies in which the third phase is a boride, an oxide, or a carbide. As can be seen, the best properties correspond to the $B_4C$–$TiB_2$–$Al_4C_3$ system, *i.e.*, again the combination of carbide and boride as secondary phases to achieve super–hard materials with improved toughness. For the fabrication of these composites, a Ti–Al intermetallic compound was used as sintering additive. This melts at ~1450 °C, thus generating a transient liquid–phase which is consumed in reacting with $B_4C$ in accordance with the reaction:

$$2B_4C+4Ti–Al+C \rightarrow 4TiB_2+Al_4C_3 \quad (2.10)$$

so that the composite material resulting from sintering is of the $B_4C$–$TiB_2$–$Al_4C_3$ type. The presence of $Al_4C_3$ in the composite is very interesting since it is a carbide which is also very light, ultra–hard, and refractory. Again, the scarcity of studies on $B_4C$–based composites using Ti–Al as sintering additive is surprising since the densification temperatures are considerably lowered, and the composites obtained exhibit an excellent combination of mechanical properties.

## $B_4C$–based systems with more than three phases

Finally, **Table 2.16** lists the results of recent work in which $B_4C$–based composite materials have been fabricated with microstructures made up of more than three phases, with a hardness of ~30 GPa and a toughness of ~6 MPa·$m^{1/2}$. As can be seen, in all three cases the resulting composite contains a certain proportion of SiC. Two of them also use nanocarbon toughening reinforcement, once again showing the convenience of adding these phases to $B_4C$ to obtain ultra–hard materials with improved toughness. Nonetheless, the properties of these systems do not surpass those of others with far simpler microstructures, such as those fabricated using $MoSi_2$ or Ti–Al as sintering additives.

**Table 2.16.** Sintering of $B_4C$–based systems with more than three phases.

| No | P | SP | ST | SC | RD (%) | H (GPa) | $K_{IC}$ (MPa·$m^{1/2}$) | Y | R |
|---|---|---|---|---|---|---|---|---|---|
| 1 | $B_4C$–SiC–$Al_4SiC_4$–$Al_8B_4C_7$–$Al_3B_{48}C_2$–$AlB_{12}$ | $B_4C$ +15wt.% SiC +3wt.% Al +1.5wt.%GPL | SPS | 1825°C, 30MPa, 5min, vacuum | ~100 | ~30.1 | ~5.9 | 2018 | [116] |
| 2 | $B_4C$–SiC–$B_2O_3$–$TiO_2$–C–$CeB_6$ | $B_4C$+ 5wt.% ($Ti_3SiC_2$ +$CeO_2$) | | 1650°C, 80MPa, 5min, vacuum | ~100 | ~28.5 | ~6.3 | 2020 | [59] |
| 3 | $B_4C$–SiC–$Y_3Al_5O_{12}$–$Y_2O_3$ | 78.5wt.% $B_4C$+ 15wt.% SiC +1.5wt.% GPLs+5wt.% $Al_2O_3/Y_2O_3$ | | 1900°C, 30MPa, 5min | ~98.6 | ~30.6 | ~5.7 | 2019 | [117] |

In summary, the present literature review has clearly revealed the scarcity of studies on sintering three–phase $B_4C$–based materials with secondary phases of the carbide–boride type, except for the SiC–$TiB_2$ combination. The existing studies do suggest that the secondary phase combinations of SiC–$MoB_2$ and $Al_4C_3$–$TiB_2$, which can be obtained using $MoSi_2$ and Ti–Al as sintering additives, respectively, are especially interesting to produce superhard materials with optimized toughness. They also suggest the convenience of incorporating nanocarbon reinforcements into the microstructure to improve toughness.

For this reason, this Doctoral Thesis was oriented in that direction, including

different studies carried out on fabricating $B_4C$ with $MoSi_2$ or Ti–Al, with or without the incorporation of GO or rGO, to obtain materials that are super–hard and toughened. This required a wide variety of materials to be fabricated and characterized, but always under a common experimental platform. In view of this, all the materials were fabricated using SPS. Only in this way was it possible to make a judicious comparison of the different results in order to extract processing guidelines. In addition, and to serve for applications that require parts with complex geometries and long curvatures (such as armours, bullet–proof vests, tribocomponents, *etc.*) and which are light, ultra–hard, and toughened, it was also intended to explore the fabrication of materials with pre–defined shapes by performing various colloidal processing and slip casting studies, and thus minimize machining tasks which otherwise would be unfeasible given the super–hardness of these materials. Finally, the mechanical characterization of the different materials fabricated was not exclusively restricted to the estimation of their hardness and toughness, but was extended to making detailed studies of the wear resistance of those that exhibit an optimal combination of properties.

## 2.3. References

[1] H.O. Pierson, Handbook of Refractory Carbides and Nitrides – Properties, Characteristics, Processing and Applications, William Andrew, 1996.

[2] A.K. Suri, C. Subramanian, J.K. Sonber, T.S.R.C. Murthy, Synthesis and Consolidation of Boron Carbide: A Review, Int. Mater. Rev. 55 (1) (2010) 4–40.

[3] K. Rasim, R. Ramlau, A. Leithe–Jasper, T. Mori, U. Burkhardt, H. Borrmann, W. Schnelle, C. Carbogno, M. Scheffler, Y. Grin, Local Atomic Arrangements and Band Structure of Boron Carbide, Angew. Chem. 130 (2018) 6238–6243.

[4] F. Thevenot, Boron carbide – a comprehensive review, J. Eur. Ceram. Soc. 6 (4) (1990) 205–225.

[5] V. Domnich, S. Reynaud, R.A. Haber, M. Chhowalla, Boron carbide: structure, properties, and stability under stress, J. Am. Ceram. Soc. 94 (11) (2011) 3605–3628.

[6] V. Candelario (2015) Procesado coloidal acuoso y sinterización con fase líquida de tribocerámicos avanzados de SiC [Tesis Doctoral, Universidad de Extremadura]. Repositorio Institucional – Dehesa.

[7] A. Wang, Q. He, C. Liu, L. Hu, T. Tian, J. Zhang, Z. Zhang, H. Wang, Z. Fu,

W. Wang, Y. Xiong, Enhanced toughness and strength of boron carbide ceramics with reduced graphene oxide fabricated by hot pressing, Ceram. Int. 46 (2020) 26511–26520.

[8] B.M. Moshtaghioun, A.L. Ortiz, D. Gómez–García, A. Domínguez–Rodríguez, Toughening of super–hard ultra–fine grained $B_4C$ densified by spark–plasma sintering via SiC addition, J. Eur. Ceram. Soc. 33 (2013) 1395–1401.

[9] G.H. Kwei, B. Morosin, Structures of the Boron–Rich Boron Carbides from Neutron Powder Diffraction: Implications for the Nature of the Inter–Icosahedral Chains, J. Phys. Chem. 100 (1996) 8031–8039.

[10] D. Gosset, S. Miro, S. Doriot, G. Victor, V. Motte, Evidence of amorphisation of $B_4C$ boron carbide under slow, heavy ion irradiation, Nucl. Instr. Meth. B 365 (2015) 300–304.

[11] C. Cheng, Kolan. M. Reddy, A. Hirata, T. Fujita, M. Chen, Structure and mechanical properties of boron–rich boron carbides, J. Eur. Ceram. Soc. 37 (2017) 4514–4523.

[12] A. Adoor, A. Awasthi, G. Subhash, Intrinsic hardness of boron carbide: Influence of polymorphism and stoichiometry, J. Am. Ceram. Soc. 103 (2020) 7127–7134.

[13] A.L. Ortiz, F. Sánchez–Bajo, F.L. Cumbrera, F. Guiberteau, The prolific polytypism of silicon carbide, J. Appl. Cryst. 46 (2013) 242–247.

[14] D. Emin, Structure and Single–Phase Regime of Boron Carbides, Phys. Rev. B 38 (1988) 6041–6055.

[15] L.M. Litz, R.A. Mercuri, Oxidation of boron carbide by air, water, and air–water mixtures at elevated temperatures, J. Electrochem. Soc. 110 (8) (1963) 921–925.

[16] F. Thevenot, Sintering of boron carbide and boron carbide silicon carbide two–phase materials and their properties, J. Nucl. Mater. 152 (1988) 154–162.

[17] J.E. Zorzi, C.A. Perottoni, J.A. H. da Jornada, Hardness and wear resistance of $B_4C$ ceramics prepared with several additives, Mater. Lett. 59 (2005) 2932–2935.

[18] N. Frage, L. Levin, M.P. Dariel, The effect of the sintering atmosphere on the densification of $B_4C$ ceramics, J. Solid State Chem. 177 (2004) 410–414.

[19] T.K. Roy, C. Subramanian, A.K. Suri, Pressureless sintering of boron carbide, Ceram. Int. 32 (2006) 227–233.

[20] H. Lee, R.F. Speyer, Pressureless sintering of boron carbide, J. Am. Ceram. Soc. 86 (9) (2003) 1468–1473.

[21] S. Wang, S. Gao, P. Xing, D. Nie, S. Yan, Y. Zhuang, Pressureless liquid–phase sintering of $B_4C$ with $MoSi_2$ as a sintering aid, Ceram. Int. 45 (2019) 13502–13508.

[22] C. Subramanian, T.K. Roy, T.S.R.Ch. Murthy, P. Sengupta, G.B. Kale, M.V. Krishnaiah, A.K. Suri, Effect of Zirconia addition on pressureless sintering of boron carbide, Ceram. Int. 34 (2008) 1543–1549.

[23] H.R. Baharvandi, A.M. Hadian, Pressureless sintering of $TiB_2$–$B_4C$ ceramic matrix composite, J. Mater. Eng. Perform. 17 (6) (2008) 838–841.

[24] C.H. Lee, C.H. Kim, Pressureless sintering and related reaction phenomena of $Al_2O_3$–doped $B_4C$, J. Mater. Sci. 27 (23) (1992) 6335–6340.

[25] A. Goldstein, Y. Yeshurun, A. Goldenberg, $B_4C$/metal boride composites derived from $B_4C$/metal oxide mixtures, J. Eur. Ceram. Soc. 27 (2–3) (2007) 695–700.

[26] S. Wang, P. Xing, S. Gao, W. Yang, Y. Zhuang, Z. Feng, Effect of in–situ formed $CrB_2$ on pressureless sintering of $B_4C$, Ceram. Int. 44 (2018) 20367–20374.

[27] B.Y. Yin, L.S. wang, Studies on activated sintering of jet milled $B_4C$ powders, Atom. Energy Sci. Technol. 37 (Suppl.) (2003) 70–72, 76.

[28] M. Khajehzadeh, N. Ehsani, H.R. Baharvandi, A. Abdollahi, M. Bahaaddini, A. Tamadon, Thermodynamical evaluation, microstructural characterization and mechanical properties of $B_4C$–$TiB_2$ nanocomposite produced by in–situ reaction of Nano–$TiO_2$, Ceram. Int. 46 (2020) 26970–26984.

[29] G. Liu, S. Chen, Y. Zhao, Y. Fu, Y. Wang, The effect of transition metal carbides MeC (Me = Ti, Zr, Nb, Ta, and W) on mechanical properties of $B_4C$ ceramics fabricated via pressureless sintering, Ceram. Int. 46 (2020) 27283–27291.

[30] G. Liu, S. Chen, Y.Zhao, Y. Fu, Y. Wang, Effect of Ti and its compounds on the mechanical properties and microstructure of $B_4C$ ceramics fabricated via pressureless sintering, Ceram. Int. 47 (2021) 13756–13761.

[31] K.A. Schwetz, W. Grellner, The influence of carbon on the microstructure and mechanical properties of sintered boron carbide, J. Less Comm. Met. 82 (1981) 37–47.

[32] H.R. Baharvandi, A.M. Hadian, H. Abdizade, N. Ehsani, Investigation on addition of talc on sintering behavior and mechanical properties of $B_4C$, J. Mater. Eng. Perform. 15 (3) (2006) 280–283.

[33] H.R. Baharvandi, A.M. Hadian, A. Abdizadeh, N. Ehsani, Investigation on

addition of $ZrO_2$–3 mol% $Y_2O_3$ powder on sintering behavior and mechanical properties of $B_4C$, J. Mater. Sci. 41 (2006) 5269–5272.

[34] S. Prochazka, B. Lake, Dense sintered boron carbide containing beryllium carbide, US patent no. 4005235, 1977.

[35] L. Levin, N. Frage, M.P. Dariel, A novel approach for the preparation of $B_4C$–based cermets, Int. J. Refract. Met. Hard Mater. 18 (2000) 131–135.

[36] M. Mashhadi, E. Taheri–Nassaj, V.M. Sglavo, Pressureless sintering of boron carbide, Ceram. Int. 36 (2010) 151–159.

[37] M. Mashhadi, E. Taheri–Nassaj, M. Mashhadi, V.M. Sglavo, Pressureless sintering of $B_4C$–$TiB_2$ composites with Al additions, Ceram. Int. 37 (2011) 3229–3235.

[38] G.B. Ghorbal, A. Tricoteaux, A. Thault, G. Louis, D. Chicot, Comparison of conventional Knoop and Vickers hardness of ceramic materials, J. Eur. Ceram. Soc. 37 (2017) 2531–2535.

[39] G.R. Anstis, P. Chantikul, B.R. Lawn, D.B. Marshall, A Critical Evaluation of Indentation Techniques for Measuring Fracture Toughness: I, Direct Crack Measurements, J. Am. Ceram. Soc. 64 (9) (1981) 533–538.

[40] R. Angers, M. Beauvy, Hot–pressing of boron carbide, Ceram. Int. 10 (2) (1983) 49–55.

[41] T. Jiang, Z. Jin, J. Yang, G. Qiao, Investigation on the preparation and machinability of the $B_4C$/BN nanocomposites by hot–pressing process, J. Mater. Proc. Technol. 209 (2009) 561–571.

[42] S. Yamada, K. Hirao, Y. Yamauchi, S. Kanzaki, $B_4C$–$CrB_2$ composites with improved mechanical properties, J. Eur. Ceram. Soc. 23 (2003) 561–565.

[43] X. Du, Z. Zhang, Y. Wang, J. Wang, W. Wang, H. Wang, and Z. Fu, Hot–Pressing Kinetics and Densification Mechanisms of Boron Carbide, J. Am. Ceram. Soc. 98 (5) (2015) 1400–1406.

[44] P. He, S. Dong, Y. Kan, X. Zhang, Y. Ding, Microstructure and mechanical properties of $B_4C$–$TiB_2$ composites prepared by reaction hot pressing using $Ti_3SiC_2$ as additive, Ceram. Int. 42 (2016) 650–656.

[45] I.T. Ostapenko, V.V. Slezov, R.V. Tarasov, N.F. Kartsev, V.P. Podtykan, Densification of boron carbide powder during hot pressing, Sov. Powder Metall. Met. Ceram. 18 (5) (1979) 312–316.

[46] D. Jianxin, Erosion wear of boron carbide ceramic nozzles by abrasive air–jets, Mater. Sci. Eng. A 408 (2005) 227–233.

[47] L.S. Dole, S. Prochazka, R.H. Doremus, Microstructural coarsening during

sintering of boron carbide, J. Am. Ceram. Soc. 72 (6) (1989) 958–966.

[48] J. Deng, J. Zhou, Y. Feng, Z. Ding, Microstructure and mechanical properties of hot–pressed $B_4C$/(W,Ti)C ceramic composites, Ceram. Int. 28 (2002) 425–430.

[49] D. Jianxin, S. Junlong, Microstructure and mechanical properties of hot–pressed $B_4C$/TiC/Mo ceramic composites, Ceram. Int. 35 (2009) 771–778.

[50] X. Zhang, Z. Zhang, W. Wang, J. Shan, H. Che, J. Mu, G. Wang, Microstructure and mechanical properties of $B_4C$–$TiB_2$–SiC composites toughened by composite structural toughening phases, J. Am. Ceram. Soc. 100 (2017) 3099–3107.

[51] M. Fajar, A. Gubarevich, R.S.S. Maki, T. Uchikoshi, T.S. Suzuki, T. Yano, K. Yoshida, Effect of $Al_2O_3$ addition on texturing in a rotating strong magnetic field and densification of $B_4C$, Ceram. Int. 45 (2019) 18222–18228.

[52] X. Du, Z. Zhang, W. Wang, H. Wang, Z. Fu, Microstructure and properties of $B_4C$–SiC composites prepared by polycarbosilane–coating/$B_4C$ powder route, J. Eur. Ceram. Soc. 34 (2014) 1123–1129.

[53] Y. Xiong, X. Du, M. Xiang, H. Wang, W. Wang, Z. Fu, Densification mechanism during reactive hot pressing of $B_4C$–$ZrO_2$ mixtures, J. Eur. Ceram. Soc. 38 (2018) 4167–4172.

[54] Y. Tan, H. Luo, H. Zhang, X. Zhou, S. Peng, Fabrication of toughened $B_4C$ composites with high electrical conductivity using MAX phase as a novel sintering aid, Ceram. Int. 42 (2016) 7347–7352.

[55] Z. Zhong, A. Yang, R. Wang, Q. Wen, Z. Zhu, G. Wang, H. Zhang, On the use of Ti–Si eutectic alloy as a novel sintering aid for $B_4C$–$TiB_2$–SiC ceramic composites, Ceram. Int. 45 (2019) 12393–12398.

[56] S. Yamada, K. Hirao, Y. Yamauchi, S. Kanzaki, Mechanical and electrical properties of $B_4C$–$CrB_2$ ceramics fabricated by liquid phase sintering, Ceram. Int. 29 (2003) 299–304.

[57] N. Cho, Z. Bao and R.F. Speyer, Density–and hardness–optimized pressureless sintered and post–hot isostatic pressed $B_4C$, J. Mater. Res. 20 (8) (2005) 2110–2116.

[58] Z.A. Munirw, D.V. Quach, Electric Current Activation of Sintering: A Review of the Pulsed Electric Current Sintering Process, J. Am. Ceram. Soc. 94 (1) (2011), 1–19.

[59] Q. Song, Z.H. Zhang, Z.Y. Hu, H. Wang, Y.F. Zhang, X.Y. Li, L.J. Liu, S.L. Li, X.W. Cheng, Mechanical properties and pre–oxidation behavior of spark

plasma sintered $B_4C$ ceramics using ($Ti_3SiC_2$+$CeO_2$/$La_2O_3$) as sintering aid, Ceram. Int. 46 (2020) 22189–22196.

[60] M. Li, W. Wang, Q. He, A. Wang, L. Hu, Z. Fu, Reduced–graphene–oxide–reinforced boron carbide ceramics fabricated by spark plasma sintering from powder mixtures obtained by heterogeneous coprecipitation, Ceram. Int. 45 (2019) 16496–16503.

[61] M. Asadikiya, C. Zhang, C. Rudolf, B. Boesl, A. Agarwal, Y. Zhong, The effect of sintering parameters on spark plasma sintering of $B_4C$, Ceram. Int. 43 (2017) 11182–11188.

[62] B. Yavas, F. Sahin, O. Yucel, G. Gollern, Effect of particle size, heating rate and CNT addition on densification, microstructure and mechanical properties of $B_4C$ ceramics, Ceram. Int. 41 (2015) 8936–8944.

[63] W.S. Rubink, V. Ageh, H. Lide, N.A. Ley, M.L. Young, D.T. Casem, E.J. Faierson, T.W. Scharf, Spark plasma sintering of $B_4C$ and $B_4C$–$TiB_2$ composites: Deformation and failure mechanisms under quasistatic and dynamic loading, J. Eur. Ceram. Soc. 41 (2021) 3321–3332.

[64] B.M. Moshtaghioun, A.L. Ortiz, D. Gómez–García, A. Domínguez–Rodríguez, Densification of $B_4C$ nanopowder with nanograin retention by spark–plasma sintering, J. Eur. Ceram. Soc. 35 (2015) 1991–1998.

[65] F. Ye, Z. Hou, H. Zhang, L. Liu, Densification and Mechanical Properties of Spark Plasma Sintered $B_4C$ with Si as a Sintering Aid, J. Am. Ceram. Soc. 93 (10) (2010) 2956–2959.

[66] M. Zhang, T. Yuan, R. Li, S. Xie, M. Wang, Q. Weng, Densification mechanisms and microstructural evolution during spark plasma sintering of boron carbide powders, Ceram. Int. 44 (2018) 3571–3579.

[67] B.M. Moshtaghioun, F.L. Cumbrera, A.L. Ortiz, M. Castillo–Rodríguez, D. Gómez–García, Additive–free superhard $B_4C$ with ultrafine–grained dense microstructures, J. Eur. Ceram. Soc. 34 (2014) 841–848.

[68] R. Belon, G. Antou, N. Pradeilles, A. Maître, D. Gosset, Mechanical behaviour at high temperature of spark plasma sintered boron carbide ceramics, Ceram. Int. 43 (2017) 6631–6635.

[69] B.M. Moshtaghioun, A.L. Ortiz, D. Gómez–García, A. Domínguez–Rodríguez, Enhancing the spark–plasma sinterability of $B_4C$ nanopowders via room–temperature methylation induced purification, J. Eur. Ceram. Soc. 36 (2016) 2843–2848.

[70] D. Ren, Q. Deng, J. Wang, Y. Li, M. Li, S. Ran, S. Du, Q. Huang,

Densification and mechanical properties of pulsed electric current sintered $B_4C$ with in situ synthesized $Al_3BC$ obtained by the molten–salt method, J. Eur. Ceram. Soc. 37 (2017) 4524–4531.

[71] K.Y. Xie, M.F. Toksoy, K. Kuwelkar, B. Zhang, J.A. Krogstad, R.A. Haber, K.J. Hemker, Effect of Alumina on the Structure and Mechanical Properties of Spark Plasma Sintered Boron Carbide, J. Am. Ceram. Soc. 97 (11) (2014) 3710–3718.

[72] A.L. Ortiz, V.M. Candelario, O. Borrero–López, F. Guiberteau, Sliding–wear resistance of pure near fully–dense $B_4C$ under lubrication with water, diesel fuel, and paraffin oil, J. Eur. Ceram. Soc. 38 (2018) 1158–1163.

[73] J. Sun, B. Niu, L. Ren, J. Zhang, L. Lei, F. Zhang, Densification and mechanical properties of boron carbide prepared via spark plasma sintering with cubic boron nitride as an additive, J. Eur. Ceram. Soc. 40 (2020) 1103–1110.

[74] S. Azuma, T. Uchikoshi, K. Yoshida, T.S. Suzuki, Fabrication of textured $B_4C$ ceramics with oriented tubal pores by strong magnetic field–assisted colloidal processing, J. Eur. Ceram. Soc. 41 (2021) 2366–2374.

[75] S.S. Rehman, W. Ji, S.A. Khan, M. Asif, Z. Fu, W. Wang, H. Wang, J. Zhang, Y. Wang, Microstructure and mechanical properties of $B_4C$ based ceramics with $Fe_3Al$ as sintering aid by spark plasma sintering, J. Eur. Ceram. Soc. 34 (2014) 2169–2175.

[76] W. Ji, R.I. Todd, W. Wang, H. Wang, J. Zhang, Z. Fu, Transient liquid phase spark plasma sintering of $B_4C$–based ceramics using Ti–Al intermetallics as sintering aid, J. Eur. Ceram. Soc. 36 (2016) 2419–2426.

[77] C. Sun, Y. Lin, Y. Wang, L. Zhu, Q. Jiang, Y. Miao, X. Chen, Effect of alumina addition on the densification of boron carbide ceramics prepared by spark plasma sintering technique, Ceram. Int. 40 (2014)12723–12728.

[78] M. Biesuza, V.M. Sglavo, Flash sintering of ceramics, J. Eur. Ceram. Soc. 39 (2019) 115–143.

[79] J. Wu, B. Niu, F. Zhang, L. Lei, J. Zhang, L. Ren, W. Wang, Z. Fu, Effect of titanium diboride on the homogeneity of boron carbide ceramic by flash spark plasma sintering, Ceram. Int. 44 (2018) 15323–15330.

[80] A. Wang, Q. He, C. Liu, L. Hu, T. Tian, Z. Zhang, Y. Xiong, W. Wang, H. Wang, Z. Fu, Microstructure and mechanical properties of boron carbide/graphene nanoplatelets composites fabricated by hot pressing, Ceram. Int. 46 (2020) 7879–7887.

[81] A. Kovalčíková, R. Sedlák, P. Rutkowski, J. Dusza, Mechanical properties of boron carbide+graphene platelet composites, Ceram. Int. 42 (2016) 2094–2098.

[82] B.M. Moshtaghioun, D. Gómez–García, A. Domínguez–Rodríguez, R.I. Todd, Grain size dependence of hardness and fracture toughness in pure near fully–dense boron carbide ceramics, J. Eur. Ceram. Soc. 36 (7) (2016) 1829–1834.

[83] G.V. Samsonov, I.M. Vinitskii, Refractory Compounds: Handbook, 2nd Edition (in russian), Metallurgiya, Moscow, 1976

[84] https://www.azom.com/properties.aspx?ArticleID=492

[85] Q. Liu, W. Han, X. Zhang, S. Wang, J. Han, Microstructure and mechanical properties of ZrB2–SiC composites, Mater. Lett. 63 (15) (2009) 1323–1325.

[86] X. Zhang, G.E. Hilmas, W.G. Fahrenholtz, Synthesis, densification, and mechanical properties of $TaB_2$, Mater. Lett. 62 (27) (2008) 4251–4253.

[87] V. Reddy, J.K. Sonber, K. Sairam, T.S.R.Ch. Murthy, S. Kumar, G.V.S. Nageswara, S. Rao, J.K. Chakravartty, Densification and mechanical properties of $CrB_2$+$MoSi_2$ based novel composites, Ceram. Int. 41 (6) (2015) 7611–7617.

[88] V. Skorokhod, M.D. Vlajic, V.D. Krstic, Mechanical properties of pressureless sintered boron carbide containing $TiB_2$ phase, J. Mater. Sci. Lett. 15 (1996) 1337–1339.

[89] Z. Liu, X. Deng, J. Li, Y. Sun, S. Ran, Effects of $B_4C$ particle size on the microstructures and mechanical properties of hot–pressed $B_4C$–$TiB_2$, Ceram. Int. 44 (2018) 21415–21420.

[90] K. Hirao, S. Sakaguchi, Y. Yamauchi, S. Kanzaki, S. Yamada, Boron carbide based sintered compact and method for preparation thereof, US patent no. 0 059 541 A1, 2005.

[91] S.G. Huang, K. Vanmeensel, O. Van der Biest, J. Vleugels, In situ synthesis and densification of submicrometer–grained $B_4C$–$TiB_2$ composites by pulsed electric current sintering, J. Eur. Ceram. Soc. 31 (2011) 637–644.

[92] N. Firshtman, S. Kalabukhov, N. Frage, Effect of boron carbide composition on its densification behavior during spark plasma sintering (SPS), Ceram. Int. 44 (2018) 21842–21847.

[93] J. Dai, J. Singh, N. Yamamoto, Fabrication and characterization of FAST sintered micro/nano boron carbide composites with enhanced fracture toughness, J. Eur. Ceram. Soc. 40 (2020) 5272–5285.

[94] https://www.americanelements.com/titanium–dioxide–13463–67–7

[95] S.G. Huang, K. Vanmeensel, J. Vleugels, Powder synthesis and densification of

ultrafine $B_4C$–$ZrB_2$ composite by pulsed electrical current sintering, J. Eur. Ceram. Soc. 34 (2014) 1923–1933.

[96] S.S. Rehman, W. Ji, Z. Fu, W. Wang, H. Wang, M. Asif, J. Zhang, In situ synthesis and sintering of $B_4C/ZrB_2$ composites from $B_4C$ and $ZrH_2$ mixtures by spark plasma, J. Eur. Ceram. Soc. 35 (2015) 1139–1145.

[97] https://www.us–nano.com/inc/sdetail/14745

[98] D. Demirskyi, Y. Sakka, O. Vasylkiv, High–Strength $B_4C$–$TaB_2$ Eutectic Composites obtained via In Situ by Spark Plasma Sintering, J. Am. Ceram. Soc. 99 (7) (2016) 2436–2441.

[99] S. M. So, W.H. Choi, K.H. Kim, J.S. Park, M.S. Kim, J. Park, Y.S. Lim, H.S. Kim, Mechanical properties of $B_4C$–SiC composites fabricated by hot–press sintering, Ceram. Int. 46 (2020) 9575–9581.

[100] Z. Zhang, X. Du, Z. Li, W. Wang, J. Zhang, Z. Fu, Microstructures and mechanical properties of $B_4C$–SiC intergranular/intragranular nanocomposite ceramics fabricated from $B_4C$, Si, and graphite powders, J. Eur. Ceram. Soc. 34 (2014) 2153–2161.

[101] S.S. Rehman, W. Ji, S.A. Khan, Z. Fun, F. Zhang, Microstructure and mechanical properties of $B_4C$ densified by spark plasma sintering with Si as a sintering aid, Ceram. Int. 41 (2015) 1903–1906.

[102] B.M. Moshtaghioun, D. Gómez–García, A. Domínguez–Rodríguez, High–temperature plastic deformation of spark plasma sintered boron carbide–based composites: The case study of $B_4C$–SiC with/without graphite (g), J. Eur. Ceram. Soc. 36 (2016) 1127–1134.

[103] X. Zhang, Z. Zhang, W. Wang, H. Che, X. Zhang, Y. Bai, L. Zhang, Z. Fu, Densification behaviour and mechanical properties of $B_4C$–SiC intergranular/intragranular nanocomposites fabricated through spark plasma sintering assisted by mechanochemistry, Ceram. Int. 43 (2017) 1904–1910.

[104] Z.A. Yas, R.A. Haber, Evaluating the role of uniformity on the properties of $B_4C$–SiC composites, Ceram. Int. 47 (2021) 4838–4844.

[105] https://www.surfacenet.de/yttrium–aluminum–garnet–y3al5o12.html

[106] X. Li, Y. Gao, W. Pan, X. Wang, L. Song, Z. Zhong, S. Wu, Fabrication and characterization of $B_4C$–based ceramic composites with different mass fractions of hexagonal boron nitride, Ceram. Int. 41 (2015) 27–36.

[107] X. Zhang, Z. Zhang, Y. Liu, A. Wang, S. Tian, W. Wang, J. Wang, High–performance $B_4C$–$TiB_2$–SiC composites with tuneable properties fabricated by reactive hot pressing, J. Eur. Ceram. Soc. 39 (2019) 2995–3002.

[108] Q. He, A. Wang, C. Liu, W. Wang, H. Wang, Z. Fu, Microstructures and mechanical properties of $B_4C$–$TiB_2$–SiC composites fabricated by ball milling and hot pressing, J. Eur. Ceram. Soc. 38 (2018) 2832–2840.

[109] Y. Wang, Q. Liu, B. Zhang, H. Zhang, Y. Jin, Z. Zhong, J. Ye, F. Ye, W. Wang, Microstructure and mechanical behaviour of transient liquid phase spark plasma sintered $B_4C$–SiC–$TiB_2$ composites from a $B_4C$–$TiSi_2$ system, Ceram. Int. 47 (2021) 10665–10671.

[110] Q. Song, Z.H. Zhang, Z.Y. Hu, S.P. Yin, H. Wang, Z.W. Ma, Microstructure and mechanical properties of super–hard $B_4C$ ceramic fabricated by spark plasma sintering with ($Ti_3SiC_2$+Si) as sintering aid, Ceram. Int. 45 (2019) 8790–8797.

[111] S.P. Yin, Z.H. Zhang, X.W. Cheng, T.J. Su, Z.Y. Hu, Q. Song, H. Wang, Spark plasma sintering of $B_4C$–$TiB_2$–SiC composite ceramics using $B_4C$, $Ti_3SiC_2$ and Si as starting materials, Ceram. Int. 44 (2018) 21626–21632.

[112] S. Sabooni, F. Karimzadeh, M.H. Abbasi, Thermodynamic aspects of nanostructured $Ti_5Si_3$ formation during mechanical alloying and its characterization, Bull. Mater. Sci. (35) (2012) 439–447.

[113] https://en.wikipedia.org/wiki/MAX_phases

[114] S. Kumar, K. Sairam, J.K. Sonber, T.S.R.C. Murthy, V. Reddy, G.V.S.N. Rao, T.S. Rao, Hot–pressing of $MoSi_2$ reinforced $B_4C$ composites, Ceram. Int. 40 (2014) 16099–16105.

[115] S. Junlong, L. Changxia, L. Hongqi, L. Bin, Effect of mechanical properties and impact angles on erosion behavior of $B_4C/TiB_2$ matrix ceramic nozzle materials, Ceram. Int. 42 (2016) 8826–8832.

[116] M. Chen, Z. Yin, J. Yuan, W. Xu, J. Ye, S. Yan, Microstructure and properties of a graphene platelets toughened boron carbide composite ceramic by spark plasma sintering, Ceram. Int. 44 (2018) 15370–15377.

[117] Z. Yin, J. Yuan, M. Chen, D. Si, C. Xu, Mechanical property and ballistic resistance of graphene platelets/$B_4C$ ceramic armor prepared by spark plasma sintering, Ceram. Int. 45 (2019) 23781–23787.

# CHAPTER 3

# Fabricating toughened super–hard $B_4C$ composites at lower temperature by transient liquid–phase assisted spark plasma sintering with $MoSi_2$ additives

Cristina Ojalvo, Fernando Guiberteau, Angel L. Ortiz*

*Departamento de Ingeniería Mecánica, Energética y de los Materiales, Universidad de Extremadura, 06006 Badajoz, Spain.*

**Corresponding author: Angel L. Ortiz, E–mail address: alortiz@unex.es; Tel: +34–924–289–300; Fax: +34–924–289–601.*

**Journal of the European Ceramic Society 39 (9) (2019), 2862–2873.**
doi: https://doi.org/10.1016/j.jeurceramsoc.2019.03.035

*Received 23 January 2019*
*Received in revised form 7 March 2019*
*Accepted 15 March 2019*

## Abstract

Toughened, super–hard $B_4C$ triplex–particulate composites were densified by spark plasma sintering with $MoSi_2$ additives (5, 10, and 15 vol.%) at temperatures in the range 1750–1850 °C at which the reference monolithic $B_4C$ ceramics are porous. It is proved that $MoSi_2$ is a reactive sintering additive that promotes densification by transient liquid–phase sintering, thus yielding fully–dense $B_4C$–$MoB_2$–SiC composites at relatively lower temperatures. Specifically, the $MoSi_2$ first reacts at moderate temperatures (<1150 °C) with part of $B_4C$ to form $MoB_2$, SiC, and Si. This last is a transient component that eventually melts (at ~1400 °C), contributing to densification by liquid–phase sintering, and then (at 1500–1700 °C) reacts with free C present in the $B_4C$ starting powders to form more SiC, after which densification continues by solid–state sintering. It is found that these $B_4C$–$MoB_2$–SiC composites are super–hard (~30 GPa), tough (~3–4 $MPa{\cdot}m^{1/2}$), and fine–grained, a combination that renders them very appealing for structural applications. Finally, research opportunities are discussed for the future microstructural design of a novel family of toughened, ultra–hard/super–hard multi–particulate composites based on $B_4C$ plus refractory borides and carbides.

# CHAPTER 4

# Ultra–low wear $B_4C$–SiC–$MoB_2$ composites fabricated at lower temperature from $B_4C$ with $MoSi_2$ additives

Víctor Zamora, Cristina Ojalvo, Óscar Borrero–López, Fernando Guiberteau, Angel L. Ortiz*

*Departamento de Ingeniería Mecánica, Energética y de los Materiales, Universidad de Extremadura, 06006 Badajoz, Spain.*

**Corresponding author: Angel L. Ortiz, E–mail address: alortiz@unex.es; Tel: +34–924–289–300; Fax: +34–924–289–601.*

**Journal of the European Ceramic Society, in press (2021)**
https://doi.org/10.1016/j.jeurceramsoc.2021.09.014

*Received 4 August 2021*
*Received in revised form 3 September 2021*
*Accepted 7 September 2021*

## Abstract

Seeking to fabricate $B_4C$ composites that are even more superhard (>30 GPa) at lower cost, $B_4C$ was transient liquid–phase assisted spark–plasma–sintered, somewhat counterintuitively, at lower temperature (<1750 °C) and with greater $MoSi_2$ aid content (>15 vol.%) than ever before. It was found that just 20 vol.% $MoSi_2$ aid enables the full densification of $B_4C$ at 1700 °C, thereby avoiding the deleterious transformation $\beta$–$MoB_2 \rightarrow \alpha$–$MoB_2$, having consumed the entire $MoSi_2$ to form $MoB_2$ and SiC. This maximizes the hardness (~33 GPa) of these novel triple–particulate $B_4C$–SiC–$MoB_2$ composites without penalizing their toughness (~4.1 $MPa{\cdot}m^{1/2}$). Also importantly, the dry sliding–wear of these novel composites was investigated for the first time, showing that they undergo only mild wear (specific wear rate of ~10–8 $mm^3/N{\cdot}m$) by plasticity–dominated two–body abrasion. Moreover, it was demonstrated that they are much more wear resistant than porous $B_4C$ monolithics fabricated under both the same and more demanding conditions, and at least as equally wear resistant as fully–dense $B_4C$ monolithics and composites fabricated under more demanding conditions.

# CHAPTER 5

# Improving the dry sliding–wear resistance of $B_4C$ ceramics by transient liquid–phase sintering

Cristina Ojalvo, Estíbaliz Sánchez–González, Fernando Guiberteau, Óscar Borrero–López, Angel L. Ortiz*

*Departamento de Ingeniería Mecánica, Energética y de los Materiales, Universidad de Extremadura, 06006 Badajoz, Spain.*

**Corresponding author: Angel L. Ortiz, E–mail address: alortiz@unex.es; Tel: +34–924–289–300; Fax: +34–924–289–601.*

**Journal of the European Ceramic Society 40 (15) (2020), 5286–5292.**
https://doi.org/10.1016/j.jeurceramsoc.2020.05.065

*Received 1 April 2020*
*Received in revised form 23 May 2020*
*Accepted 26 May 2020*

## Abstract

A critical comparison is made between the dry sliding–wear resistance of a $B_4C$ composite fabricated by transient liquid–phase sintering with Ti–Al intermetallic additive and two reference monolithic $B_4C$ ceramics fabricated by solid–state sintering. It is shown that, as a consequence of its full densification and super–hardness, the $B_4C$ composite is, despite containing secondary phases, markedly more wear resistant (significantly lower coefficient of friction, specific wear rate, worn volume, and wear damage) than the reference monolithic $B_4C$ ceramic fabricated under identical spark–plasma–sintering (SPS) conditions, and at least as wear resistant as the reference monolithic $B_4C$ ceramic fabricated at much higher SPS temperature. In all materials, wear is nonetheless mild and occurred by two–body abrasion dominated by plastic deformation at the micro–contact level plus, in the porous reference monolithic $B_4C$ ceramic, three–body abrasion dominated by fracture. Implications for the lower–cost manufacture of superhard $B_4C$ tribocomponents are discussed.

# CHAPTER 6

# Manufacturing $B_4C$ parts with Ti–Al intermetallics by aqueous colloidal processing

Cristina Ojalvo[a], Rodrigo Moreno[b], Fernando Guiberteau[a], Angel L. Ortiz[a,*]

[a] *Departamento de Ingeniería Mecánica, Energética y de los Materiales, Universidad de Extremadura, 06006 Badajoz, Spain.*
[b] *Instituto de Cerámica y Vidrio, Consejo Superior de Investigaciones Científicas, Madrid, 28049, Spain.*

**Corresponding author: Angel L. Ortiz, E–mail address: alortiz@unex.es; Tel: +34–924–289–300; Fax: +34–924–289–601.*

**Journal of the European Ceramic Society 40 (2) (2020), 226–233.**
doi: https://doi.org/10.1016/j.jeurceramsoc.2019.10.002

*Received 11 June 2019*
*Received in revised form 30 September 2019*
*Accepted 1 October 2019*

## Abstract

The aqueous colloidal processing of submicrometre $B_4C$ powder (~0.6 μm) with coarse Ti–Al powder (~40 μm) as sintering additive was investigated. Firstly, by measuring the zeta potential, pHs were identified that promote the individual colloidal stability of the $B_4C$ and Ti–Al particles as well as their co–dispersion in water with two different deflocculants (one anionic and the other cationic). It was found that the anionic and cationic deflocculants shift the isoelectric points of $B_4C$ and Ti–Al to more acidic and more basic pHs, respectively, making their co–dispersion possible at neutral pH. And secondly, by means of rheological studies, conditions were identified (sonication time, deflocculant type, and deflocculant content) that at quasi–neutral pH yield $B_4C$+Ti–Al shear–thinning concentrated suspensions (30 vol.% total solids) with low viscosity and small hysteresis loop. Interestingly, those deflocculated with the cationic polyelectrolyte had better rheological behaviour, being also less viscous and almost non–thixotropic. These suspensions were freeze–dried, obtaining powder mixtures that were compacted by conventional spark plasma sintering (SPS), and also slip–cast, obtaining robust green pieces that were densified by pressureless SPS. The two $B_4C$ composites thus obtained are superhard, with Vickers hardnesses greater than 30 GPa.

# CHAPTER 7

# Transient liquid–phase assisted spark–plasma sintering and dry sliding wear of $B_4C$ ceramics fabricated from $B_4C$ nanopowders

Cristina Ojalvo[a], Victor Zamora[a], Rodrigo Moreno[b], Fernando Guiberteau[a], Angel L. Ortiz[a,*]

[a] Departamento de Ingeniería Mecánica, Energética y de los Materiales, Universidad de Extremadura, 06006 Badajoz, Spain.
[b] Instituto de Cerámica y Vidrio, Consejo Superior de Investigaciones Científicas, Madrid, 28049, Spain.

**Corresponding author: Angel L. Ortiz, E–mail address: alortiz@unex.es; Tel: +34–924–289–300; Fax: +34–924–289–601.*

**Journal of the European Ceramic Society 41 (3) (2020), 1869–1877.**
doi: https://doi.org/10.1016/j.jeurceramsoc.2020.10.058

*Received 8 October 2020*
*Received in revised form 23 October 2020*
*Accepted 25 October 2020*

## Abstract

With the motivation of developing $B_4C$ composites with superior wear resistance for tribological applications, an ultrafine–grained (~200—300 nm) $B_4C$ composite was fabricated, characterized microstructurally, and tested mechanically and tribologically. First, a well–dispersed powder mixture of $B_4C$ nanopowders (~40 nm) with coarse Ti–Al powders (~38 μm) as transient liquid–phase sintering additives was environmentally–friendly prepared by aqueous colloidal processing, optimized by measurements of the zeta potential of dilute suspensions and rheological studies of concentrated suspensions. Second, the powder mixture obtained by freeze–drying was densified by spark–plasma sintering (SPS), identifying the optimal SPS temperature (1850 °C) by measurements of density, hardness, and toughness. Third, the dry sliding–wear behaviour of the optimal superhard $B_4C$ composite (~31.5 GPa) was investigated by pin–on–disk tests and observations of the worn surface, determining its specific wear rate (~$4.4{\cdot}10^{-8}$ $mm^3/(N{\cdot}m)$) as well as wear mode (two–body abrasion) and mechanism (plastic deformation). And lastly, the wear behaviour of the ultrafine–grained $B_4C$ composite was compared with that of a reference fine–grained

~0.7–0.9 μm) $B_4C$ composite, finding that both have the same mode and mechanism of wear but with the former being more resistant than the latter (~$2.3 \cdot 10^7$ *vs* $1.9 \cdot 10^7$ $(N \cdot m)/mm^3$). Implications for the fabrication of $B_4C$ tribocomponents with greater superior wear resistance are discussed.

# CHAPTER 8

# Processing of orthotropic and isotropic superhard $B_4C$ composites reinforced with reduced graphene oxide

Cristina Ojalvo[a], Rodrigo Moreno[b], Fernando Guiberteau[a], Angel L. Ortiz[a,*]

[a] *Departamento de Ingeniería Mecánica, Energética y de los Materiales, Universidad de Extremadura, 06006 Badajoz, Spain.*
[b] *Instituto de Cerámica y Vidrio, Consejo Superior de Investigaciones Científicas, Madrid, 28049, Spain.*

**Corresponding author: Angel L. Ortiz, E–mail address: alortiz@unex.es; Tel: +34–924–289–300; Fax: +34–924–289–601.*

**Journal of the European Ceramic Society 40 (9) (2020), 3406–3413.**
doi: https://doi.org/10.1016/j.jeurceramsoc.2020.02.027

*Received 26 December 2019*
*Received in revised form 11 February 2020*
*Accepted 12 February 2020*

## Abstract

A fabrication route based on aqueous colloidal processing plus transient liquid–phase assisted spark–plasma–sintering (SPS) with Ti–Al additives is described for the environmentally friendly obtention of superhard $B_4C$ composites reinforced with reduced graphene oxide (rGO) having orthotropic and isotropic microstructures. It is shown that the former, which have coarse rGO platelets preferentially aligned perpendicular to the SPS pressing direction, can be prepared from mixtures of $B_4C$ and Ti–Al particles with a source of thick, large rGO nanoplatelets by imposing smooth co–dispersion conditions to avoid platelet reexfoliation and fragmentation. The latter, which have fine rGO platelets randomly oriented, can be fabricated from mixtures of $B_4C$ and Ti–Al particles with a source of thin, small rGO nanoplatelets by applying intensive sonication to promote platelet reexfoliation and fragmentation during co–dispersion. Finally, it is shown that these orthotropic and isotropic $B_4C$/ rGO composites are equally superhard, and that, as expected, their microstructures interact differently with the cracks. Finally, this processing route is simple, and easily adaptable/extensible to make other ceramic/rGO composites with orthotropic and isotropic microstructures.

# CHAPTER 9

# Pressureless ultrafast sintering of near–net–shaped superhard isotropic $B_4C$/rGO composites with Ti–Al additives

Cristina Ojalvo[a], Rodrigo Moreno[b], Fernando Guiberteau[a], Angel L. Ortiz[a,*]

[a] *Departamento de Ingeniería Mecánica, Energética y de los Materiales, Universidad de Extremadura, 06006 Badajoz, Spain.*
[b] *Instituto de Cerámica y Vidrio, Consejo Superior de Investigaciones Científicas, Madrid, 28049, Spain.*

**Corresponding author: Angel L. Ortiz, E–mail address: alortiz@unex.es; Tel: +34–924–289–300; Fax: +34–924–289–601.*

**Journal of the European Ceramic Society 40 (12) (2020), 4354–4360.**
doi: https://doi.org/10.1016/j.jeurceramsoc.2020.05.033

*Received 16 April 2020*
*Received in revised form 11 May 2020*
*Accepted 12 May 2020*

## Abstract

Superhard composites of $B_4C$ reinforced with randomly–oriented reduced graphene oxide (rGO) nanoplatelets are manufactured by a near–net–shape fabrication route based on three successive steps. Firstly, aqueous colloidal processing is used for the environmentally–friendly preparation of a semi–concentrated multi–component slurry ($B_4C$ as main component, Ti–Al as sintering additive, and rGO as toughening reinforcement), who se suitability for wet shaping is demonstrated by rheological measurements. Secondly, slip casting is used to produce robust green parts with shapes on demand and microstructures free of macro– and micro–defects. And thirdly, pressureless spark–plasma sintering (PSPS) is used for the ultrafast and energy–efficient densification of the green parts with shape retention. Measurements of shrinkage and hardness, as well as the microstructural observations, are used to identify suitable PSPS temperatures leading to obtaining isotropic $B_4C$/rGO composites that are superhard and almost twice as tough as the monolithic $B_4C$ ceramics.

# CHAPTER 10

# Aqueous tape casting of super–hard $B_4C$ laminates with rGO–enriched reinforcing interlayers

Cristina Ojalvo [a], Marcos Ayllón[b], Angel L. Ortiz[a], Rodrigo Moreno[b],*

[a] *Departamento de Ingeniería Mecánica, Energética y de los Materiales, Universidad de Extremadura, 06006 Badajoz, Spain.*
[b] *Instituto de Cerámica y Vidrio, Consejo Superior de Investigaciones Científicas, Madrid, 28049, Spain.*

**Corresponding author: Rodrigo Moreno, E–mail address: rmoreno@icv.csic.es*

**Journal of the European Ceramic Society 41 (3) (2021), 5457–5465**
https://doi.org/10.1016/j.jeurceramsoc.2021.05.001

*Received 24 February 2021*
*Received in revised form 26 April 2021*
*Accepted 01 May 2021*

## Abstract

Superhard $B_4C$ parts with microarchitectures constituted by ceramic layers and evenly–spaced rGO–enriched reinforcing interlayers were fabricated for the first time. To this end, a concentrated slurry of $B_4C$ with its Ti–Al sintering additive was first prepared by aqueous colloidal processing, optimizing its total solids loading and content of both binder and plasticizer to obtain, by tape casting, handleable and flexible green tapes. A semidilute aqueous suspension of $B_4C$ with Ti–Al and abundant GO was also prepared to dip–coat those greentapes with a GO–enriched layer, optimizing the withdrawal rate and the dipping time. The bare and GO–coated $B_4C$+Ti–Al tapes were then sequentially laminated, thus yielding green multilayered laminates that finally were appropriately debinded and densified by spark plasma sintering. Vickers indentation tests demonstrated that these multilayered laminates are superhard (~31 GPa), and that their rGO–enriched reinforcing interlayers are effective in arresting crack propagation.

# CHAPTER 11

## Summary of results

The objective of the present Doctoral Thesis was to develop a new generation of ultra–hard $B_4C$–based composites by transient liquid–phase assisted spark–plasma sintering (SPS). To that end, a series of eight interconnected studies, each of them constituting a Chapter of this Doctoral Thesis, were carried out. Below, a list is presented summarizing the most important results from this Doctoral Thesis, separated by Chapters:

With regard to Chapter 3, devoted to the "**fabrication of toughened super–hard $B_4C$ composites at lower temperature by transient liquid–phase assisted spark plasma sintering with $MoSi_2$ additives**", it is worth summarizing that:

1. Toughened, super–hard $B_4C$ triplex–particulate composites were densified by SPS with $MoSi_2$ additives (5, 10, and 15 vol.%) at temperatures in the range 1750–1850 °C at which the reference monolithic $B_4C$ ceramics are porous. It was proved that $MoSi_2$ is a reactive sintering additive that promotes densification by transient liquid–phase sintering, thus yielding fully–dense $B_4C$–$MoB_2$–SiC composites at relatively lower temperatures. Specifically, the $MoSi_2$ first reacts at moderate temperatures (<1150 °C) with part of $B_4C$ to form $MoB_2$, SiC, and Si. This last is a transient component that eventually melts (at ~1400 °C), contributing to densification by liquid–phase sintering, and then (at 1500–1700 °C) reacts with free C present in the $B_4C$ starting powders to form more SiC, after which densification continues by solid–state sintering. It was found that these $B_4C$–$MoB_2$–SiC composites are super–hard (~30 GPa), tough (~3–4 $MPa{\cdot}m^{1/2}$), and fine–grained, a combination that renders them very appealing for structural applications. Finally, research opportunities were discussed for the future microstructural design of a novel family of toughened, ultra–hard/super–hard multi–particulate composites based on $B_4C$ plus refractory borides and carbides.

With regard to Chapter 4, devoted to the "**ultra–low wear $B_4C$–SiC–$MoB_2$ composites fabricated at lower temperature from $B_4C$ with $MoSi_2$ additives**", it is worth summarizing that:

2. Seeking to fabricate $B_4C$ composites that are even more superhard (>30 GPa) at lower cost, $B_4C$ was transient liquid–phase assisted spark–plasma–sintered, somewhat counterintuitively, at lower temperature (<1750 °C) and with greater $MoSi_2$ aid content (>15 vol.%) than ever before. It was found that just 20 vol.% $MoSi_2$ aid enables the full densification of $B_4C$ at 1700 °C, thereby avoiding the deleterious transformation $\beta$–$MoB_2 \rightarrow \alpha$–$MoB_2$, having consumed the entire $MoSi_2$ to form $MoB_2$ and SiC. This maximizes the hardness (~33 GPa) of these novel triple–particulate $B_4C$–SiC–$MoB_2$ composites without penalizing their toughness (~4.1 MPa·$m^{1/2}$). Also importantly, the dry sliding–wear of these novel composites was investigated for the first time, showing that they undergo only mild wear (specific wear rate of ~10–8 $mm^3$/N·m) by plasticity–dominated two–body abrasion. Moreover, it was demonstrated that they are much more wear resistant than porous $B_4C$ monolithics fabricated under both the same and more demanding conditions, and at least as equally wear resistant as fully–dense $B_4C$ monolithics and composites fabricated under more demanding conditions.

With regard to Chapter 5, devoted to "**improving the dry sliding–wear resistance of $B_4C$ ceramics by transient liquid–phase sintering**", it is worth summarizing that:

3. A critical comparison was made between the dry sliding–wear resistance of a $B_4C$ composite fabricated by transient liquid–phase sintering with Ti–Al intermetallic additive and two reference monolithic $B_4C$ ceramics fabricated by solid–state sintering. It was shown that, as a consequence of its full densification and super–hardness, the $B_4C$ composite is, despite containing secondary phases, markedly more wear resistant (significantly lower coefficient of friction, specific wear rate, worn volume, and wear damage) than the reference monolithic $B_4C$ ceramic fabricated under identical SPS conditions, and at least as wear resistant as the reference monolithic $B_4C$ ceramic fabricated at much higher SPS temperature. In all materials, wear is nonetheless mild and occurred by two–body abrasion dominated by plastic deformation at the micro–contact level plus, in the porous reference monolithic $B_4C$ ceramic, three–body abrasion dominated by fracture. Implications for the lower–cost manufacture of superhard $B_4C$ tribocomponents were discussed.

With regard to Chapter 6, devoted to "**manufacturing $B_4C$ parts with Ti–Al intermetallics by aqueous colloidal processing**", it is worth summarizing that:

4. The aqueous colloidal processing of submicrometre $B_4C$ powder (~0.6 μm) with coarse Ti–Al powder (~40 μm) as sintering additive was investigated. Firstly, by measuring the zeta potential, pHs were identified that promote the individual colloidal stability of the $B_4C$ and Ti–Al particles as well as their co–dispersion in water with two different deflocculants (one anionic and the other cationic). It was found that the anionic and cationic deflocculants shift the isoelectric points of $B_4C$ and Ti–Al to more acidic and more basic pHs, respectively, making their co–dispersion possible at neutral pH. And secondly, by means of rheological studies, conditions were identified (sonication time, deflocculant type, and deflocculant content) that at quasi–neutral pH yield $B_4C$+Ti–Al shear–thinning concentrated suspensions (30 vol.% total solids) with low viscosity and small hysteresis loop. Interestingly, those deflocculated with the cationic polyelectrolyte had better rheological behaviour, being also less viscous and almost non–thixotropic. These suspensions were freeze–dried, obtaining powder mixtures that were compacted by conventional SPS, and also slip–cast, obtaining robust green pieces that were densified by pressureless SPS. The two $B_4C$ composites thus obtained are superhard, with Vickers hardnesses greater than 30 GPa.

With regard to Chapter 7, devoted to the "**transient liquid–phase assisted spark–plasma sintering and dry sliding wear of $B_4C$ ceramics fabricated from $B_4C$ nanopowders**", it is worth summarizing that:

5. With the motivation of developing $B_4C$ composites with superior wear resistance for tribological applications, an ultrafine–grained (~200–300 nm) $B_4C$ composite was fabricated, characterized microstructurally, and tested mechanically and tribologically. First, a well–dispersed powder mixture of $B_4C$ nanopowders (~40 nm) with coarse Ti–Al powders (~38 μm) as transient liquid–phase sintering additives was environmentally–friendly prepared by aqueous colloidal processing, optimized by measurements of the zeta potential of dilute suspensions and rheological studies of concentrated suspensions. Second, the powder mixture obtained by freeze–drying was densified by SPS, identifying the optimal SPS temperature (1850 °C) by measurements of density, hardness, and toughness. Third, the dry sliding–wear behaviour of the

optimal superhard $B_4C$ composite (~31.5 GPa) was investigated by pin–on–disk tests and observations of the worn surface, determining its specific wear rate (~$4.4 \cdot 10^{-8}$ $mm^3/(N \cdot m)$) as well as wear mode (two–body abrasion) and mechanism (plastic deformation). And lastly, the wear behaviour of the ultrafine–grained $B_4C$ composite was compared with that of a reference fine–grained (~0.7–0.9 μm) $B_4C$ composite, finding that both have the same mode and mechanism of wear but with the former being more resistant than the latter (~$2.3 \cdot 10^7$ *vs* $1.9 \cdot 10^7$ $(N \cdot m)/mm^3$). Implications for the fabrication of $B_4C$ tribocomponents with greater superior wear resistance were discussed.

With regard to Chapter 8, devoted to the "**processing of orthotropic and isotropic superhard $B_4C$ composites reinforced with reduced graphene oxide**", it is worth summarizing that:

6. A fabrication route based on aqueous colloidal processing plus transient liquid–phase assisted SPS with Ti–Al additives was described for the environmentally friendly obtention of superhard $B_4C$ composites reinforced with reduced graphene oxide (rGO) having orthotropic and isotropic microstructures. It was shown that the former, which have coarse rGO platelets preferentially aligned perpendicular to the SPS pressing direction, can be prepared from mixtures of $B_4C$ and Ti–Al particles with a source of thick, large rGO nanoplatelets by imposing smooth co–dispersion conditions to avoid platelet re–exfoliation and fragmentation. The latter, which have fine rGO platelets randomly oriented, can be fabricated from mixtures of $B_4C$ and Ti–Al particles with a source of thin, small rGO nanoplatelets by applying intensive sonication to promote platelet re–exfoliation and fragmentation during co–dispersion. Finally, it was shown that these orthotropic and isotropic $B_4C$/rGO composites are equally superhard, and that, as expected, their microstructures interact differently with the cracks. Finally, this processing route is simple, and easily adaptable/extensible to make other ceramic/rGO composites with orthotropic and isotropic microstructures.

With regard to Chapter 9, devoted to the "**pressureless ultrafast sintering of near–net–shaped superhard isotropic $B_4C$/rGO composites with Ti–Al additives**", it is worth summarizing that:

7. Superhard composites of $B_4C$ reinforced with randomly–oriented reduced

graphene oxide (rGO) nanoplatelets were manufactured by a near–net–shape fabrication route based on three successive steps. Firstly, aqueous colloidal processing was used for the environmentally–friendly preparation of a semi–concentrated multi–component slurry ($B_4C$ as main component, Ti–Al as sintering additive, and rGO as toughening reinforcement), whose suitability for wet shaping was demonstrated by rheological measurements. Secondly, slip casting was used to produce robust green parts with shapes on demand and microstructures free of macro– and micro–defects. And thirdly, pressureless spark–plasma sintering (PSPS) was used for the ultrafast and energy–efficient densification of the green parts with shape retention. Measurements of shrinkage and hardness, as well as the microstructural observations, were used to identify suitable PSPS temperatures leading to obtaining isotropic $B_4C$/rGO composites that are superhard and almost twice as tough as the monolithic $B_4C$ ceramics.

With regard to Chapter 10, devoted to the "**aqueous tape casting of super–hard $B_4C$ laminates with rGO–enriched reinforcing interlayers**", it is worth summarizing that:

8. Superhard $B_4C$ parts with microarchitectures constituted by ceramic layers and evenly–spaced rGO–enriched reinforcing interlayers were fabricated for the first time. To this end, a concentrated slurry of $B_4C$ with its Ti–Al sintering additive was first prepared by aqueous colloidal processing, optimizing its total solids loading and content of both binder and plasticizer to obtain, by tape casting, handleable and flexible green tapes. A semi–dilute aqueous suspension of $B_4C$ with Ti–Al and abundant GO was also prepared to dip–coat those green tapes with a GO–enriched layer, optimizing the withdrawal rate and the dipping time. The bare and GO–coated $B_4C$+Ti–Al tapes were then sequentially laminated, thus yielding green multilayered laminates that finally were appropriately debinded and densified by SPS. Vickers indentation tests demonstrated that these multilayered laminates are superhard (~31 GPa), and that their rGO–enriched reinforcing interlayers are effective in arresting crack propagation.

# CHAPTER 12

# Conclusions

In this Doctoral Thesis, a number of different but interconnected studies were conducted, all aimed at developing a new generation of ultra–hard $B_4C$–based composites by transient liquid–phase (TLP) assisted spark–plasma sintering (SPS). Below, a list is presented of the most relevant conclusions to be drawn from this Doctoral Thesis, separated by studies:

With regard to the study entitled "**fabrication of toughened super–hard $B_4C$ composites at lower temperature by transient liquid–phase assisted spark plasma sintering with $MoSi_2$ additives**", it is worth concluding that:

1. $MoSi_2$ additives can be used to fabricate $B_4C$ multi–particulate composites with superior toughness (~3–4 $MPa{\cdot}m^{1/2}$) and super–high hardness (~30 GPa) by SPS at lower temperatures.
2. Increasing $MoSi_2$ addition (in the range 5–15 vol.%) benefits $B_4C$ sinterability and toughness, without penalizing its hardness.
3. The $B_4C$–$MoSi_2$ powder mixtures lead to $B_4C$–$MoB_2$–SiC triple–particulate composites with fine–grained microstructures because $MoSi_2$ acts as a reactive sintering additive that promotes the lower–temperature densification of $B_4C$ by TLP sintering.
4. $MoSi_2$ first reacts at moderate temperatures (<1150 °C) with part of $B_4C$ to form $MoB_2$, SiC, and Si. This last is a transient component that eventually melts (at ~1400 °C), contributing to densification by liquid–phase sintering, and then (at 1500–1700 °C) reacts with free C present in the $B_4C$ starting powders to form more SiC, after which densification continues by solid–state sintering.

With regard to the study entitled "**ultra–low wear $B_4C$–SiC–$MoB_2$ composites fabricated at lower temperature from $B_4C$ with $MoSi_2$ additives**", it is worth concluding that:

5. The $B_4C$ composites TLP–SPSed with $MoSi_2$ aids are triplex–particulate ceramics whose microstructure consists of a matrix of $B_4C$ grains containing both $MoB_2$+SiC clusters and single SiC grains uniformly dispersed.

6. Only with 20 vol.% $MoSi_2$ aid can $B_4C$ be TLP–SPSed at 1700 °C, thus avoiding the deleterious transformation β–$MoB_2$→α–$MoB_2$, having been consumed all the $MoSi_2$ in forming SiC and $MoB_2$. It therefore yields $B_4C$–SiC–$MoB_2$ composites that are more superhard (~33 GPa) and with the same fracture toughness as the toughest (~4.1 MPa·$m^{1/2}$).
7. $MoSi_2$ aid content below or above 20 vol.% lessens the super–hardness of these $B_4C$–SiC–$MoB_2$ composites (~30 GPa). The former is because the higher SPS temperatures required for full densification promote the occurrence of the transformation β–$MoB_2$→α–$MoB_2$, and the latter because there is less of the hard $B_4C$ phase and more of the soft β–$MoB_2$ and β–SiC (plus unreacted $MoSi_2$ or $MoSi_2$+Si which are even softer).
8. Under conditions of dry sliding, $B_4C$–SiC–$MoB_2$ composites with the optimal 20 vol% $MoSi_2$ undergo mild wear, and show increased wear resistance (by a factor of 4.4) over $B_4C$ monoliths SPSed under the same conditions, attributable to their lower porosity (and attendant lower CoF and greater hardness).
9. The wear mechanism of the fully–dense $B_4C$–SiC–$MoB_2$ composites is mainly plastic deformation at the asperity level, while $B_4C$ monoliths SPSed under the same conditions show additional grain pull–out due to microfracture at porosity defects.

With regard to the study entitled "**improving the dry sliding–wear resistance of $B_4C$ ceramics by transient liquid–phase sintering**", it is worth concluding that:

10. Ti–Al additives promote the lower–temperature densification of $B_4C$, yielding superhard $B_4C$ composites with finer microstructures than those of their superhard near–fully dense monolithic $B_4C$ counterparts.
11. The $B_4C$ composites have an excellent dry sliding–wear resistance that comparatively exceeds by a factor of two those of the monolithic $B_4C$ ceramics fabricated under the same conditions, attributable to their total densification and much greater hardness.
12. The $B_4C$ composites have, despite containing secondary phases, dry sliding–wear resistances that are at least as great as those of the monolithic $B_4C$ ceramics near–fully densified at much higher temperatures, which is attributable to their total densification, slightly greater hardness, and finer microstructures.

13. The $B_4C$ ceramics and composites undergo mild wear, which occurs principally by two–body abrasion dominated by plastic deformation at the micro–contact level. If porous, monolithic $B_4C$ ceramics also exhibit three–body abrasion dominated by fracture.
14. Owing to the easier processing, lower cost, and enhanced wear resistance, $B_4C$ composites fabricated by TLP sintering are advantageous for tribological applications compared with monolithic $B_4C$ ceramics.

With regard to the study entitled "**manufacturing $B_4C$ parts with Ti–Al intermetallics by aqueous colloidal processing**", it is worth concluding that:

15. A procedure of aqueous colloidal processing was developed for the environmentally friendly preparation of well dispersed concentrated suspensions, and therefrom powder mixtures, of commercially available powders of submicrometre $B_4C$ (~0.6 μm) with coarse Ti–Al (~40 μm) as TLP sintering additive.
16. $B_4C$ has little colloidal stability in water, requiring very basic pH (*i.e.*, pH >10) for its individual dispersion. Ti–Al has greater colloidal stability than $B_4C$, requiring quasi–neutral pH or above (*i.e.*, pH >7.5).
17. The addition of cationic (*i.e.*, PEI) or anionic (*i.e.*, PAA) deflocculants simultaneously improves the colloidal stability of both $B_4C$ and Ti–Al, making their co–dispersion possible at neutral pH (pH ≤9 and pH ≥5 when using PEI and PAA, respectively).
18. Although the concentrated suspensions (*i.e.*, 30 vol.% total solids) can be deflocculated with PEI or PAA, the former are less viscous and thixotropic/rheopexic than the latter and have the desirable shear–thinning rheological behaviour, being therefore preferable for obtaining both powder mixtures by freeze–drying and green pieces by slip–casting
19. It is feasible to fabricate superhard $B_4C$ composites from these powder mixtures by conventional SPS with pressure or from the slip–cast (green) pieces by SPS without pressure.

With regard to the study entitled "**transient liquid–phase assisted spark–plasma sintering and dry sliding wear of $B_4C$ ceramics fabricated from $B_4C$ nanopowders**", it is worth concluding that:

20. Optimal conditions have been identified for the environmentally friendly

fabrication of these composites by aqueous colloidal processing and TLP assisted SPS with Ti–Al additives. The processing variables optimized were the deflocculant content (7 wt.% PEI), the total solids loading (25 vol.%), the dispersion mode (non–sonication), and the SPS temperature (1850 °C).

21. These ultrafine–grained $B_4C$ composites were observed to be superhard (~31.5 GPa) and relatively tough (~4 $MPa{\cdot}m^{1/2}$), as is also the case of the fine–grained counterparts.
22. Dry sliding wear of these composites, whether they have ultrafine or fine grain sizes, was shown to occur by two–body abrasion dominated by plastic deformation (ploughing), and as a result of their superhardness, they undergo only very mild wear with negligible grain pullout.
23. The ultrafine–grained $B_4C$ composite was demonstrated to be more wear resistant than its fine–grained counterpart, with lower specific wear rate (~$4.4{\cdot}10^{-8}$ *vs* $5.2{\cdot}10^{-8}$ $mm^3/(N{\cdot}m)$ under the present testing conditions) and less damage. The microstructural refinement resulting from the use of starting $B_4C$ nanopowders is therefore a processing guideline to follow in order to obtain $B_4C$ tribocomponents with even greater wear resistance.

With regard to the study entitled "**processing of orthotropic and isotropic superhard $B_4C$ composites reinforced with reduced graphene oxide**", it is worth concluding that:

24. A simple processing route combining aqueous colloidal processing with TLP assisted SPS has been developed that is customizable to obtain both orthotropic and isotropic $B_4C$/rGO composites, controllably.
25. In this route, the orthotropic $B_4C$/rGO composites are obtained by using a source of coarse rGO platelets and imposing smooth codispersion conditions during aqueous colloidal processing to avoid their re–exfoliation/re–fragmentation.
26. Contrarily, the isotropic $B_4C$/rGO composites are obtained by using a source of fine rGO platelets and imposing intensive co–dispersion conditions to ensure their re–exfoliation/re–fragmentation.
27. Both types of $B_4C$/rGO composites are equally superhard (~31–32 GPa). Nonetheless, the orthotropic composites exhibit marked toughening and virtually no toughening for cracks propagating perpendicularly and in parallel to the rGO reinforcements, respectively. The isotropic composites exhibit

however moderate toughening for any crack.

With regard to the study entitled "**pressureless ultrafast sintering of near–net–shaped superhard isotropic $B_4C$/rGO composites with Ti–Al additives**", it is worth concluding that:

28. It is possible to fabricate superhard, toughened $B_4C$/rGO composites with isotropic microstructures by combining aqueous slip casting and SPS without pressure.
29. The former enables the environmentally–friendly preparation of slurries with shear–thinning rheological behaviour, low viscosity, and little thixotropy to obtain robust green parts with shape on demand and microstructures free of macro– and micro–defects, and the latter enables the ultrafast densification of these green parts while retaining their shape.
30. By the measurement of shrinkages and hardnesses, as well as by microstructural observations, sintering temperatures were identified suitable for obtaining superhard isotropic $B_4C$/rGO composites with enhanced fracture toughness relative to monolithic $B_4C$ ceramics.

With regard to the study entitled "**aqueous tape casting of super–hard $B_4C$ laminates with rGO–enriched reinforcing interlayers**", it is worth concluding that:

31. An optimal concentrated slurry has been formulated (32 vol.% total solids, and 15 wt.% of both PVA binder and PEG plasticizer) that allows the obtention of green $B_4C$+Ti–Al tapes with appropriate handleability, flexibility, and surface finish.
32. A semi–dilute suspension of $B_4C$ with Ti–Al and abundant GO (30 vol.%) has been formulated that allows the green $B_4C$+Ti–Al tapes to be dip–coated with a GO–enriched layer.
33. Green multilayered parts have been shaped by sequentially laminating bare and GO–coated $B_4C$+Ti–Al tapes to the desired final thickness.
34. Optimal conditions have been identified for the thermal debinding of these green laminates.
35. It has been demonstrated that the SPS–ed laminates are superhard (~31 GPa), and that their rGO–enriched reinforcing interlayers are able to arrest crack propagation. Further studies are however necessary to elucidate the reinforcing mechanisms.

# CHAPTER 13

# Conclusiones

En esta Tesis Doctoral se han llevado a cabo una serie de estudios diferentes pero interconectados, todos ellos encaminados a desarrollar una nueva generación de compuestos ultraduros basados en $B_4C$ mediante sinterización asistida con fase líquida transitoria (FLT) por descarga eléctrica pulsada (SPS). A continuación se presenta una relación de las conclusiones más relevantes que se extraen de esta Tesis Doctoral, separadas por estudios:

Con respecto al estudio titulado **"fabricación de compuestos $B_4C$ superduros y más tenaces a menor temperatura mediante sinterización por descarga eléctrica pulsada asistida por fase líquida transitoria con aditivos de $MoSi_2$"**, cabe concluir que:

1. Se pueden usar aditivos de $MoSi_2$ para fabricar compuestos multiparticulados basados en $B_4C$ con tenacidad mejorada (~3–4 $MPa{\cdot}m^{1/2}$) y súper–alta dureza (~30 GPa) mediante SPS a menores temperaturas.
2. Aumentar la cantidad de $MoSi_2$ (en el rango de 5 a 15% en volumen) beneficia la sinterabilidad y la tenacidad del $B_4C$, sin penalizar su dureza.
3. Las mezclas de polvos de $B_4C$–$MoSi_2$ dan lugar a compuestos triple–particulados de $B_4C$–$MoB_2$–SiC con microestructuras de grano fino porque el $MoSi_2$ actúa como un aditivo de sinterización reactivo que promueve la densificación a menor temperatura del $B_4C$ mediante sinterización con FLT.
4. El $MoSi_2$ primero reacciona a temperaturas moderadas (<1150 °C) con parte del $B_4C$ para formar $MoB_2$, SiC y Si. Este último es un compuesto transitorio que finalmente funde (a ~1400 °C), contribuyendo a la densificación mediante sinterización con fase líquida, y luego (a 1500–1700 °C) reacciona con el C libre presente en los polvos de partida de $B_4C$ para formar más SiC, después de lo cual la densificación continúa mediante sinterización en estado sólido.

Con respecto al estudio titulado **"compuestos de $B_4C$–SiC–$MoB_2$ de ultrabajo desgaste fabricados a menor temperatura a partir de $B_4C$ con aditivos de $MoSi_2$"**, cabe concluir que:

5. Los compuestos de $B_4C$ fabricados mediante SPS asistida con FLT con aditivos de $MoSi_2$ son cerámicos triple–particulados cuya microestructura consiste en una matriz de granos de $B_4C$ que contienen tanto cúmulos de $MoB_2$+SiC como granos individuales de SiC uniformemente dispersos.
6. Sólo con un 20% en volumen de aditivos de $MoSi_2$ es posible densificar $B_4C$ mediante SPS asistida con FLT a 1700 °C, evitando de este modo la deteriorante transformación $\beta$–$MoB_2 \rightarrow \alpha$–$MoB_2$, habiendo consumido todo el $MoSi_2$ en la formación de SiC y $MoB_2$. Por lo tanto, se obtienen así compuestos de $B_4C$–SiC–$MoB_2$ más superduros (~33 GPa) y con la misma tenacidad a fractura que el que más (~4.1 MPa·$m^{1/2}$).
7. Los contenidos de aditivo de $MoSi_2$ por debajo y por encima del 20% en volumen disminuyen la superdureza de estos compuestos de $B_4C$–SiC–$MoB_2$ (~30 GPa). Lo primero porque las mayores temperaturas de SPS requeridas para la completa densificación promueven que ocurra la transformación $\beta$–$MoB_2 \rightarrow \alpha$–$MoB_2$, y lo segundo porque hay menos fase de $B_4C$ duro y más $\beta$–$MoB_2$ y SiC blandos (además de $MoSi_2$ sin reaccionar o $MoSi_2$+Si que son incluso más blandos).
8. En condiciones de deslizamiento en seco, los compuestos de $B_4C$–SiC–$MoB_2$ con el 20% en volumen óptimo de $MoSi_2$ sufren un desgaste moderado, y tienen una mayor resistencia al desgaste (por un factor de 4.4) que los monolitos de $B_4C$ fabricados mediante SPS en las mismas condiciones, lo cual se debe a su menor porosidad (con el correspondiente menor coeficiente de fricción y mayor dureza).
9. El mecanismo de desgaste de los compuestos de $B_4C$–SiC–$MoB_2$ completamente densos es esencialmente deformación plástica al nivel de las asperezas, mientras que los monolitos de $B_4C$ fabricados mediante SPS en las mismas condiciones sufren también arranque de grano debido a microfractura en los defectos de porosidad.

Con respecto al estudio titulado **"mejorando la resistencia al desgaste por deslizamiento en seco de los cerámicos de $B_4C$ mediante sinterización con fase líquida transitoria"**, cabe concluir que:

10. Los aditivos de Ti–Al promueven la densificación a menor temperatura del $B_4C$, produciendo compuestos de $B_4C$ superduros con microestructuras más finas que las de los homólogos superduros y casi completamente densos de

$B_4C$ monolítico.

11. Los compuestos de $B_4C$ tienen una excelente resistencia al desgate por deslizamiento en seco que comparativamente es mayor por un factor dos a los cerámicos monolíticos de $B_4C$ fabricados en las mismas condiciones, lo que se atribuye a su total densificación y mucha mayor dureza.
12. Los compuestos de $B_4C$, a pesar de contener fases secundarias, presentan resistencias al desgaste por deslizamiento en seco que son al menos tan elevadas como las de los cerámicos monolíticos de $B_4C$ casi completamente densificados a temperaturas mucho mayores, lo que se debe a su completa densificación, a su dureza algo mayor y a sus microestructuras más finas.
13. Los cerámicos y los compuestos de $B_4C$ sufren un desgaste moderado, que se produce principalmente por abrasión de dos cuerpos dominada por deformación plástica a nivel de los microcontactos. Si son porosos, los cerámicos monolíticos de $B_4C$ también experimentan abrasión de tres cuerpos dominada por fractura.
14. Debido a su procesado más sencillo, su menor coste y su mayor resistencia al desgaste, los compuestos de $B_4C$ fabricados mediante sinterización con FLT son más recomendables para aplicaciones tribológicas que los cerámicos monolíticos de $B_4C$.

Con respecto al estudio titulado **"fabricando piezas de $B_4C$ con intermetálicos de Ti–Al mediante procesado coloidal acuoso"**, cabe concluir que:

15. Se ha desarrollado una ruta de procesado coloidal acuoso para la preparación ecológica de suspensiones concentradas bien dispersas y, a partir de ellas, mezclas de polvos comerciales de $B_4C$ de tamaño submicrométrico (~0.6 μm) con Ti–Al de tamaño grueso (~40 μm) como aditivo de sinterización con FLT.
16. El $B_4C$ tiene poca estabilidad coloidal en agua, requiriendo un pH muy básico (es decir, pH >10) para su dispersión individual. El Ti–Al tiene mayor estabilidad coloidal que el $B_4C$, y requiere un pH casi neutro o superior (es decir, pH >7.5).
17. La incorporación de defloculantes catiónicos (es decir, PEI) o aniónicos (es decir, PAA) mejora simultáneamente la estabilidad coloidal del $B_4C$ y del Ti–Al, permitiendo su co–dispersión a pH neutro (pH ≤9 y pH ≥5 si se utiliza PEI y PAA, respectivamente).
18. Aunque se pueden deflocular las suspensiones concentradas (es decir, 30% vol.

de sólidos totales) tanto con PEI como con PAA, las primeras son menos viscosas y tixotrópicas/reopéxicas que las segundas y tienen el deseado comportamiento reológico fluidificante, por lo que son entonces preferibles para obtener tanto mezclas de polvos por liofilización como piezas verdes por moldeo fluido.

19. Es posible fabricar compuestos superduros de $B_4C$ a partir de estas mezclas de polvos mediante SPS convencional con presión o a partir de las piezas coladas (verdes) mediante SPS sin presión.

Con respecto al estudio titulado **"sinterización por descarga eléctrica pulsada asistida con fase líquida transitoria y desgaste por deslizamiento en seco de cerámicos de $B_4C$ fabricados a partir de nanopolvos de $B_4C$"**, cabe concluir que:

20. Se han identificado las condiciones óptimas para la fabricación ecológica de estos compuestos mediante procesado coloidal acuoso y SPS asistida con FLT con aditivos de Ti–Al. Las variables de procesado optimizadas han sido el contenido de defloculante (7% en peso de PEI), la carga de sólidos totales (25% en volumen), el modo de dispersión (sin sonicación) y la temperatura de SPS (1850 °C).
21. Se ha observado que estos compuestos de $B_4C$ de grano ultrafino son superduros (~31.5 GPa) y relativamente tenaces (~4 $MPa \cdot m^{1/2}$), como también es el caso de los homólgos de grano fino.
22. Se ha demostrado que el desgaste por deslizamiento en seco de estos materiales compuestos, ya sean de tamaño de grano ultrafino o fino, ocurre mediante abrasión de dos cuerpos dominada por deformación plástica ("arado"), y que como resultado de su superdureza sólo sufren un desgaste muy moderado casi sin apenas arranque de grano.
23. Se ha demostrado que el compuesto de $B_4C$ de grano ultrafino es más resistente al desgaste que su homólogo de grano fino, con una velocidad específica de desgaste menor (~$4.4 \cdot 10^{-8}$ frente a $5.2 \cdot 10^{-8}$ $mm^3/(N \cdot m)$ en las presentes condiciones de ensayo) y con menos daño. El refinamiento microestructural resultante del uso de nanopolvos de $B_4C$ de partida es, por tanto, una directriz de procesado a seguir para obtener tribocomponentes de $B_4C$ con una resistencia al desgaste aún mayor.

Con respecto al estudio titulado **"procesado de compuestos de $B_4C$**

**superduros ortotrópicos e isotrópicos reforzados con óxido de grafeno reducido"**, cabe concluir que:

24. Se ha desarrollado una ruta de procesado sencilla que combina el procesado coloidal acuoso con SPS asistida con FLT que se puede adaptar para obtener compuestos de $B_4C$/rGO tanto ortotrópicos como isotrópicos, de manera controlada.
25. En esta ruta, los compuestos ortotrópicos de $B_4C$/rGO se obtienen utilizando una fuente de plaquetas de rGO gruesas e imponiendo condiciones suaves de codispersión durante el procesado coloidal acuoso para evitar su reexfoliación/refragmentación.
26. Por el contrario, los compuestos isotrópicos de $B_4C$/rGO se obtienen utilizando una fuente de plaquetas finas de rGO e imponiendo condiciones intensas de codispersión para asegurar su reexfoliación/refragmentación.
27. Ambos tipos de compuestos de $B_4C$/rGO son igualmente superduros (~31–32 GPa). No obstante, los compuestos ortotrópicos son marcadamente más tenaces e igualmente tenaces para fisuras que se propagan perpendicularmente y en paralelo a los refuerzos de rGO, respectivamente. Sin embargo, los compuestos isotrópicos presentan una moderada mejora de tenacidad para cualquier fisura.

Con respecto al estudio titulado **"sinterización ultrarrápida sin presión de compuestos de $B_4C$/rGO superduros e isotrópicos de casi forma final con aditivos de Ti–Al"**, cabe concluir que:

28. Es posible fabricar compuestos de $B_4C$/rGO superduros y más tenaces con microestructuras isotrópicas combinando el moldeo por colado acuoso con SPS sin presión.
29. El primero permite la preparación ecológica de suspensiones con comportamiento reológico fluidizante, baja viscosidad y poca tixotropía para obtener piezas verdes robustas con forma a demanda y microestructuras libres de macro y microdefectos, y el segundo permite la densificación ultrarrápida de estas piezas verdes preservando su forma.
30. Mediante la medida de contracciones y durezas, y gracias también a las observaciones microestructurales, se han podido identificar las temperaturas de sinterización adecuadas para obtener compuestos de $B_4C$/rGO superduros e isotrópicos con mayor tenacidad a fractura que los cerámicos monolíticos de

$B_4C$.

Con respecto al estudio titulado **"moldeo acuoso en cinta de laminados de $B_4C$ superduros con intercapas reforzantes enriquecidas con rGO"**, cabe concluir que:

31. Se ha formulado una barbotina concentrada óptima (32% en volumen de sólidos totales y 15% en peso de aglutinante de PVA y plastificante de PEG) que permite la obtención de cintas verdes de $B_4C$+Ti–Al con una adecuada manejabilidad, flexibilidad y acabado superficial.
32. Se ha formulado una suspensión semidiluida de $B_4C$ con Ti–Al y abundante GO (30% en volumen) que permite recubrir por inmersión las cintas verdes de $B_4C$+Ti–Al con una capa enriquecida con GO.
33. Se han conformado piezas verdes multicapa laminando secuencialmente cintas de $B_4C$+Ti–Al sin recubrir y recubiertas con GO hasta obtener el grosor final deseado.
34. Se han identificado las condiciones óptimas para la eliminación térmica de los orgánicos de estos laminados verdes.
35. Se ha demostrado que los laminados fabricados mediante SPS son superduros (~31 GPa) y que sus capas intercapas reforzantes enriquecidas con rGO son capaces de detener la propagación de fisuras. Sin embargo, son necesarios más estudios para identificar los mecanismos de refuerzo.